gwerth mewn gwahaniaeth
delivering on distinction

Morlais Project
Environmental Statement

Chapter 7: Metocean Conditions and Coastal Processes

Volume III

Applicant: Menter Môn Morlais Limited

Document Reference: PB5034-ES-007

Chapter 7: Metocean Conditions and Coastal Processes

Author: Royal HaskoningDHV

Morlais Document No.:	Status:	Version No:	Date:
MOR/RHDHV/APP/0010	Final	F3.0	July 2019

[Page left intentionally blank]

gwerth mewn gwahaniaeth
delivering on distinction

Morlais Project
Environmental Statement

Appendix 7.1: Morlais Demonstration Zone Tidal Resource Modelling (HR Wallingford, 2019)

Volume III

Applicant: Menter Môn Morlais Limited

Document Reference: PB5034-ES-007

Chapter 7: Metocean Conditions and Coastal Processes

Appendix 7.1: Morlais Demonstration Zone Tidal Resource Modelling (HR Wallingford, 2019)

Morlais Document No.:	Status:	Version No:	Date:
MOR/RHDHV/APP/0010	Final	F3.0	July 2019

[Page left intentionally blank]

HR Wallingford
Working with water

Morlais Demonstration Zone

Tidal Resource Modelling

DEM8387-RT001-R01-00 February 2019

Document information

Document permissions	Confidential - client
Project number	DEM8387
Project name	Morlais Demonstration Zone
Report title	Tidal Resource Modelling
Report number	RT001
Release number	R01-00
Report date	February 2019
Client	Menter Môn
Client representative	James Orme
Project manager	Robert Abernethy
Project director	Graham Siggers

Document authorisation

Prepared	Approved	Authorised
M. S. Turnbull	Robert Abernethy	

Document history

Date	Release	Prepared	Approved	Authorised	Notes
22 Feb 2019	01-00	MST	RMA	GBS	Scenario 4 added, report no updated to DEM8387 from DEM7958
19 May 2017	05-00	MST	AJC	GBS	Flood / ebb speed difference plots updated
18 May 2017	04-00	MST	AJC	GBS	Mean speed plots added plus responding to client comments.
05 May 2017	03-00	MST	AJC	GBS	
28 April 2017	02-00	MST	AJC	GBS	
13 Apr 2017	01-00	MST	AJC	GBS	

Executive Summary

The Morlais Demonstration Zone (MDZ) is situated to the west of Holy Island on the Isle of Anglesey. The MDZ will incorporate multiple tidal current turbine array projects from different project owners and with different technologies. Each will occupy a sub-zone which is a geographically defined area of seabed and will have a stated maximum capacity.

Interactions between projects will be governed by an agreement, which among other things will include details on the permitted levels of energy extraction for each project. The current form of agreement governing project interactions is the Welsh Waters Operators Agreement as provided by The Crown Estate. Owing to the close proximity of projects within the MDZ a specific Inter-Operators Agreement is being drafted which aims to manage the interactions in tidal energy resource extractions.

This study was commissioned to provide a baseline assessment of the effects of resource extraction on the level of resource available to adjacent projects. The study is undertaken in line with the resource assessment standard as defined in IEC TS 62600-201:2015.

A very high resolution 2D finite element model was set up, calibrated and applied to simulate the effects of four scenarios, with installed capacities of 60MW, 120MW, approximately 180MW and approximately 240MW of tide stream devices and assess the potential interactions between subzones. Up to 408 turbines were modelled and the potential resource extraction and resulting effects on flow speeds and average power density were assessed.

A generic turbine power and thrust curve was assumed for this study, together with a specific configuration of the multiple arrays of tide stream devices. It is understood that the effect on neighbouring subzones will be reassessed through modelling, as part of the obligations under the Inter Operators Agreement, when specific plans for installations in subzones become clearer (specific turbine devices and array configurations and locations).

Contents

Tables

1. Introduction

The Morlais Demonstration Zone (MDZ) is situated to the west of Holy Island on the Isle of Anglesey. The MDZ will incorporate multiple tidal current turbine array projects from different project owners and with different technologies. Each will occupy a sub-zone (a geographically defined area of seabed) and will have a stated maximum capacity. Figure 1.1 shows the MDZ and eight subzones.

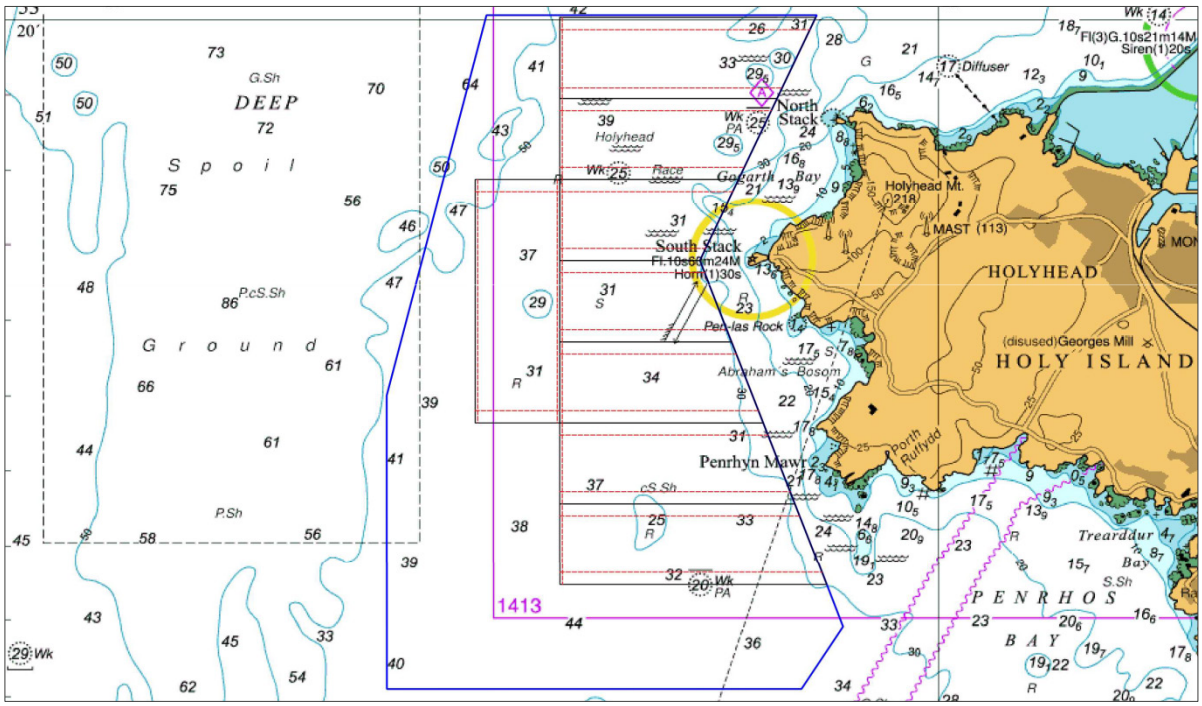

Figure 1.1: Morlais Demonstration Zone (MDZ), showing the eight proposed Sub-Zones
Source: UKHO (Chart), Menter Môn (Sub-Zones)

Interactions between projects will be governed by an agreement, which among other things will include details on the permitted levels of energy extraction for each project. The current form of agreement governing project interactions is the Welsh Waters Operators Agreement as provided by The Crown Estate. Owing to the close proximity of projects within the MDZ a specific Inter-Operators Agreement is being drafted which aims to manage the interactions in tidal energy resource extractions.

The present study was commissioned to provide a baseline assessment of the effects of resource extraction on the level of resource available to adjacent projects. The study is undertaken in line with the resource assessment standard as defined in IEC TS 62600-201:2015.

The results of the study will enable detailed discussions between project developers around the quantitative aspects of the agreements concerning the interactions of projects and a detailed understanding of the resource available.

2. Measured data

2.1. Overview

Acoustic Doppler Current Profiler (ADCP) data were provided by Morlais Energy / Menter Môn, courtesy of Open Hydro, for two positions close to Anglesey (North Wales, UK). The positions of the ADCP instruments are given in Table 2.1 below.

Table 2.1: Acoustic Doppler Current Profiler Locations

Position number	Latitude (decimal degrees)	Longitude (decimal degrees)
1	53.304132 N	4.713689 W
2	53.297777 N	4.715579 W

Source: Partrac survey for Open Hydro (November - December 2014)

The data were provided in the form of raw binary files (more than 1 Gb in size), as downloaded from the RDI/Teledyne ADCP instruments. The instruments have been set to record samples (ensembles) every second over a period of approximately 40 days.

A suite of toolboxes, some developed by HR Wallingford and other externally (including the freely available RDADCP and T-Tide toolboxes available at https://www.eoas.ubc.ca/~rich/) were used to allows portions of the data to be processed to a specified averaging interval. An averaging interval of 60 seconds was used to process the current velocities and water depths data. The current velocity data were then depth averaged following the IEC TS 62600-201 guidelines.

2.2. Review

Visual inspection of the currents at different depths in the water column indicates that the currents do not show flows with significant 3D structure and appear similar to a logarithmic velocity profile as assumed in 2D models.

2.2.1. Position 1

The data at position 1 has a break of about 24 hours on 7 and 8 December 2014, during the building up of the so called “weather bomb” extreme event that occurred on 9-10 December 2014 (http://www.metoffice.gov.uk/learning/learn-about-the-weather/weather-phenomena/weather-bomb). This gap in the data splits the measurement period available to the harmonic analysis into smaller periods, less than adequate when following the IEC TS 62600-201 guidelines. For this reason it is necessary to exercise some caution in comparing the flow model with the analysed tidal constituent data and tidal synthesis.

2.2.2. Position 2

Depths recorded by the ADCP at position 2 show a tidal range that is almost half of that expected. It was assumed that this was likely caused by an incorrect calibration of the ADCP pressure sensor.

To overcome this problem, the range (distance) to the water surface from the instrument transducer was located using the peak in the range-scaled beam-average acoustic backscatter of the four ADCP beams.

Sub-bin accuracy was achieved using a simple Gaussian fit to the bins either side of the peak in intensity. This method appeared to work well for the latter half of the data record (after 9 December 2014), but was noisy before this time. The good data period was then used to derive a linear fit relationship between the pressure sensor and the acoustically derived range to the water surface (Figure 2.1). This linear fit was then applied to the pressure data to give a recalibrated pressure sensor depth reading, which was then used to recalculate the depth averaged velocities for the entire record at position 2.

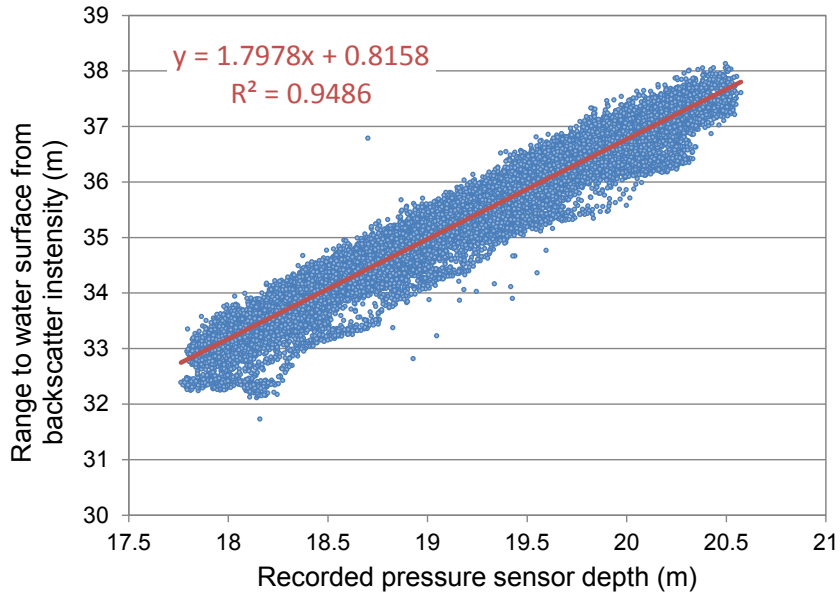

Figure 2.1: Linear relationship used to recalibrate the pressure sensor at ADCP position 2

Source: OpenHydro / HR Wallingford

In addition, the currents at position 2 contained erroneous, noisy data over a period at the start of the record until about 23 November 2014. Removing these data gaps shortened the measurement period available to the harmonic analysis. Subsequent data at position 2 appeared to be satisfactory.

2.2.3. Review conclusion

It was found that the gap in the data at position 1 and the erroneous data early in the record at position 2 made it harder to obtain sufficiently good quality tidal analysis and synthesis to be strictly following the IEC TS 62600-201 guidelines to the letter. For this reason, it is necessary to exercise some caution during the calibration and validation phases of the project in comparing the flow model results directly with the analysed tidal constituent data and tidal synthesis.

2.3. Site characterisation

The processed ADCP current velocities and water depths data are shown in Figure 2.2 and Figure 2.3 below together with the tidal analysis (based on T-Tide, available at https://www.eoas.ubc.ca/~rich/).

The measurement period includes three spring tides periods and two neap tide periods.

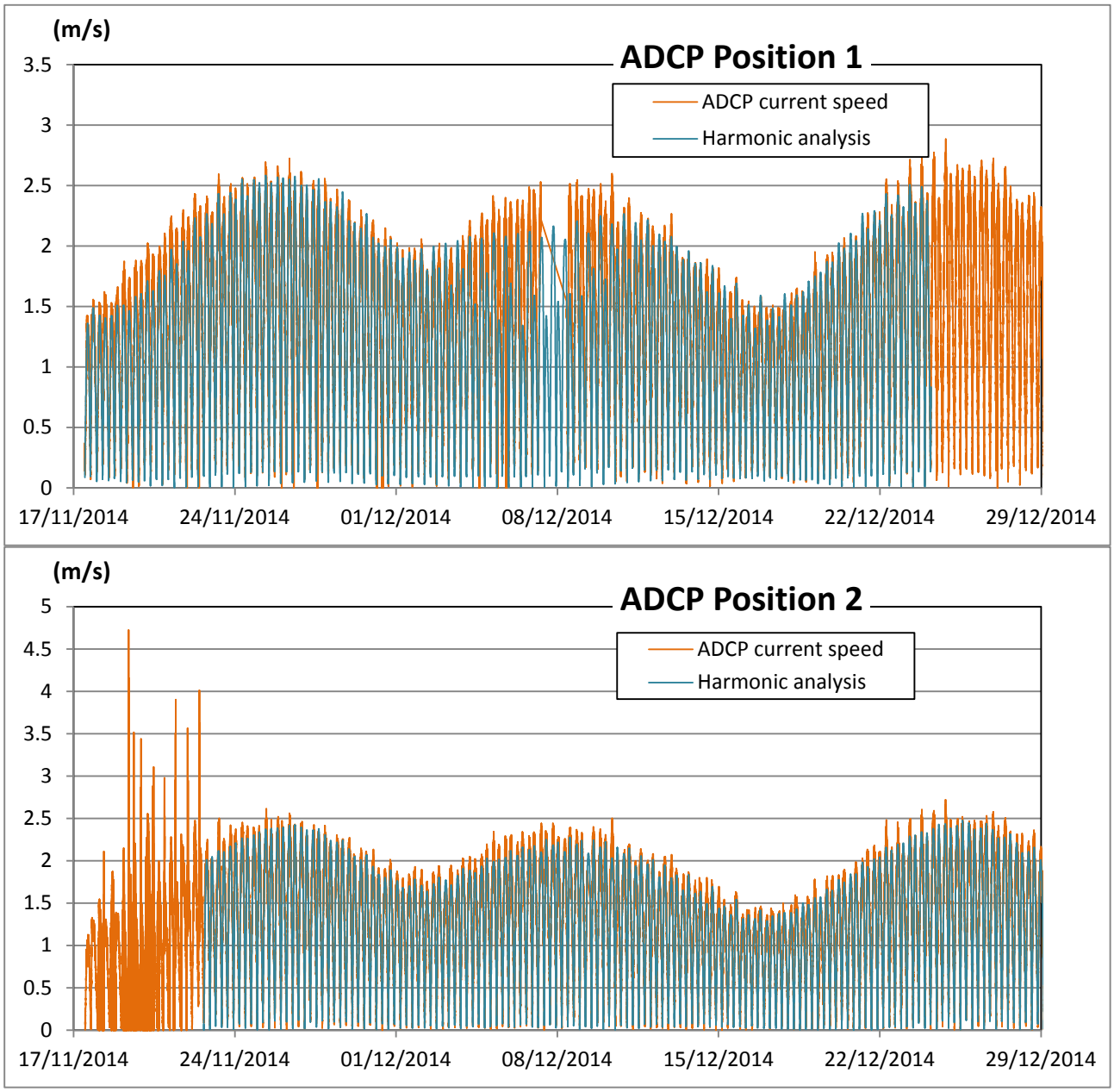

Figure 2.2: Comparison of predicted and measured current speed at ADCP position 1 and 2

Source: OpenHydro / HR Wallingford

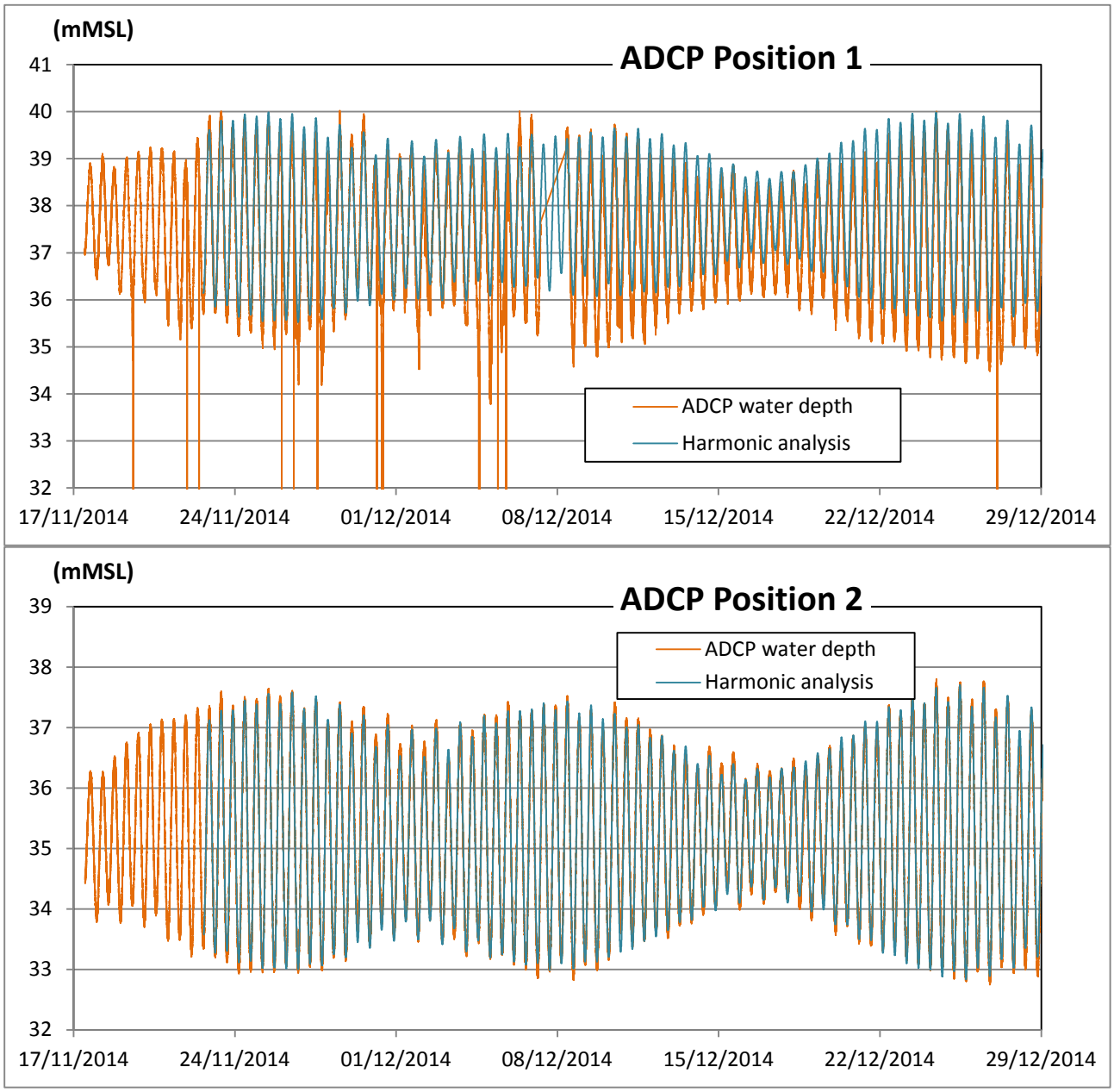

Figure 2.3: Comparison of predicted and measured water depth at ADCP position 1 and 2

Source: OpenHydro / HR Wallingford

It can be seen that the tidal analysis at position 1 is giving poor results for the spring period around the gap in the data at 7-8 December 2014. At position 2 the tidal synthesis seems to be satisfactory having excluded the initial period of noisy data. This means that the synthesis at position 2 can be used for model calibration and extrapolation to longer periods.

For all comparative tables and figures in this report, “observed” relates therefore to synthesised data for position 2, and un-synthesised data for position 1.

3. Model set-up

3.1. Overview

The modelling is based on HR Wallingford's existing and well validated Irish Sea tidal flow model. This existing model is based on the 2D depth averaged flow component of the open source TELEMAC suite of scientific solvers, TELEMAC-2D. It has previously been used to provide rely-upon information for projects for various industries (nuclear, renewable energy) and ministries (defence, infrastructure), whether for assessment, development or consent approvals.

It is considered that such 2D flow modelling is satisfactory for the purpose of this project as currents in the area of interest are relatively strong (above 2 m/s) and stratification is not expected. In addition, a review of the measured data provided by Open Hydro confirms that the vertical current profile at the two locations appears to be in line with a typical logarithmic velocity profile with depth (see Section 2).

3.1.1. Model resolution

The existing model resolution of the Irish Sea model (see Figure 3.1) has been enhanced specifically for this project to a grid resolution of 10 m around the areas of anticipated turbine deployments in the MDZ (see Figure 3.2).

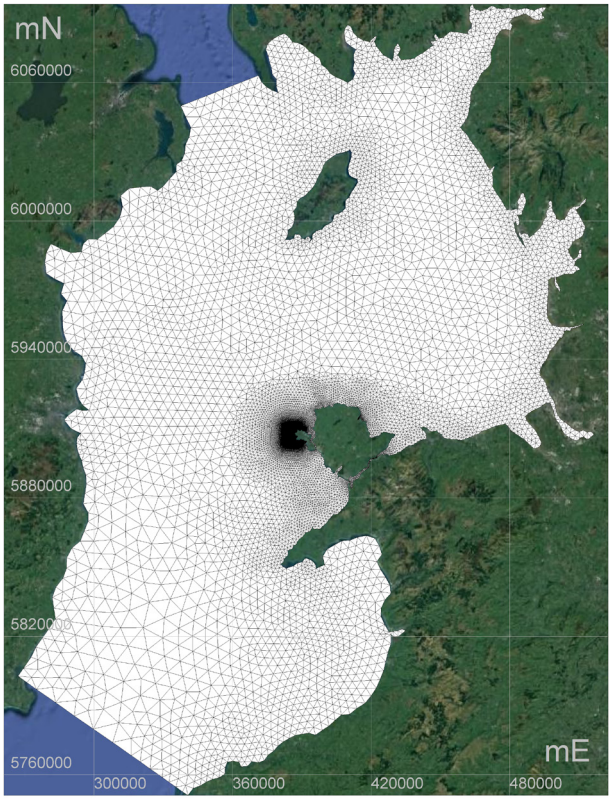

Figure 3.1: Extent of model mesh

Figure 3.2: Refined model mesh, Scenarios 1 to 3

The refinement allows for turbines to be represented individually so as to limit possible uncertainties that would be associated with a parameterisation of an array of turbines. The anticipated positioning of the turbines is clearly identified on Figure 3.2 (darker / denser mesh resolution).

For Scenario 4 (see Section 4.2), which was commissioned after the modelling of the first three developed scenarios was complete, the mesh was further refined to allow for representation of additional turbines in the northernmost and southernmost sub-zones. The refined mesh for Scenario 4 is shown in Figure 3.3.

Figure 3.3: Refined model mesh, Scenario 4

3.1.2. Model bathymetry

Refined bathymetry data were delivered by SeaZone (part of HR Wallingford) based on their Trudepth points data product, which itself is based on various UK Hydrographic Office surveys, supplemented by Charted Points data where required. Local bathymetry survey data provided by Menter Môn have also been incorporated in the final seabed mapping. The survey data were received in OD. The TruDepth, Charted Points and UKHO data were received in CD and were converted to OD by subtracting 3.05 m (the conversion for Holyhead).

Similarly to the above figures, Figure 3.4 shows the extent of the model bathymetry and Figure 3.5 the refined model bathymetry. The later also shows the MDZ as dotted lines.

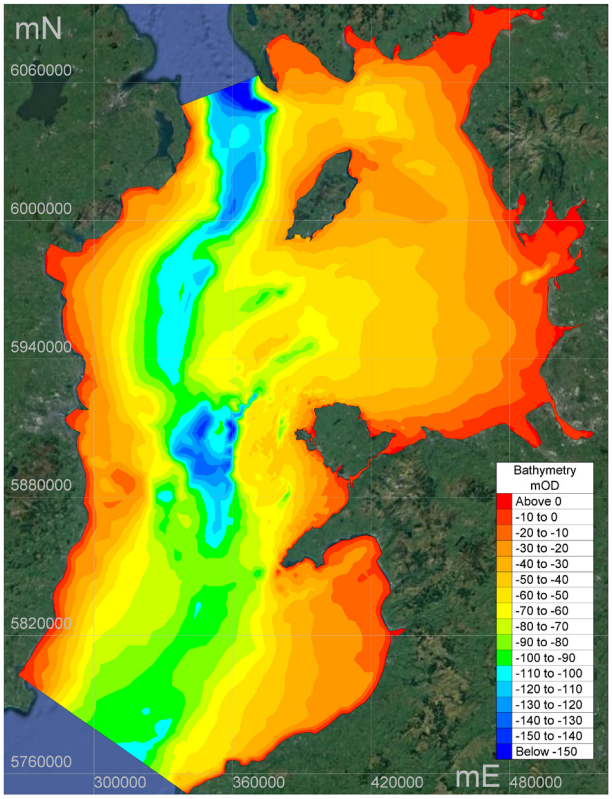

Figure 3.4: Extent of model bathymetry

Source: Menter Môn / UKHO / SeaZone

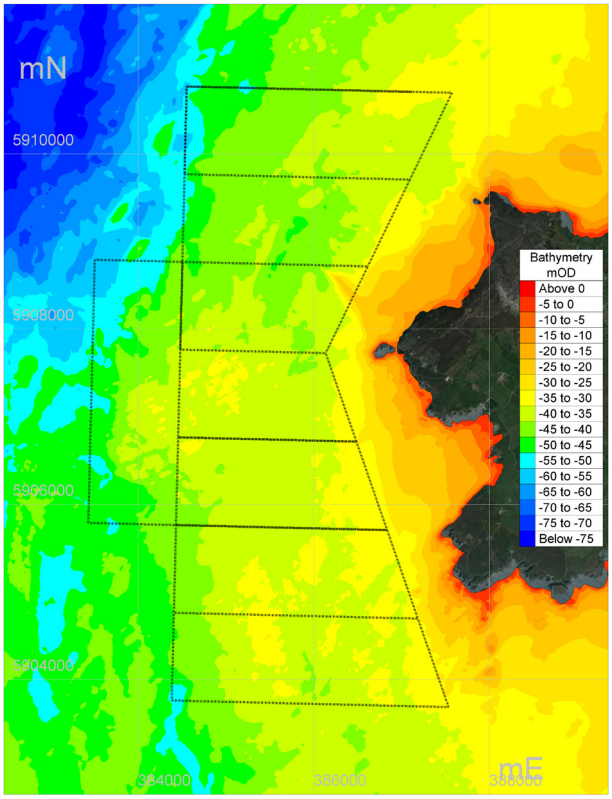

Figure 3.5: Refined model bathymetry

Source: Menter Môn / UKHO / SeaZone

3.1.3. Model boundaries

The 2D model is driven only through its open boundaries, where the model extent opens up to the St George's Channel and the North Channel (south and north of the Irish Sea respectively). Tidal water levels have been computed based on the 12 harmonics available from the high resolution TPXO tidal model dataset distributed by the Oregon State University (http://volkov.oce.orst.edu/tides/tpxo8_atlas.html).

3.2. Model calibration / validation / verification

The period considered for the calibration and validation exercise corresponds to the ADCP measurement period. The model has been run for a 44 day period starting at 0:00 hrs on 15 November 2014. The model calibration and validation exercise follows the IEC TS 62600-201 guidelines for as far as it is possible to do so given the uncertainties on the measured data (see Section 2).

3.2.1. Model calibration

The most uncertain and influential factor in a 2D modelling exercise is the nature of the seabed, specifically how the nature of the seabed influence the flows, current velocities and water depths throughout the model extent. This is parameterised as a bed friction term, which is calibrated until the model compares favourably with observations. The model was calibrated by varying the bed friction formulation (Nikuradse bed roughness length) to give close reproduction of tidal gauge data synthesised from the C-Map dataset (MIKE C- Map, DHI Water & Environment, Denmark.) at the following sites (see location map in Figure 3.6).

- Gladstone Dock
- Port St Mary
- Workington
- Barmouth
- Holyhead
- Trearddur Bay.

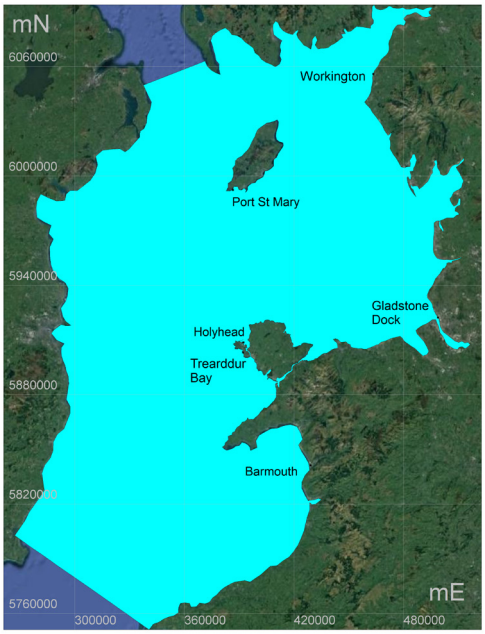

Figure 3.6: Model calibration gauges

A comparison of the model results at the end of the calibration exercise to the measured water levels at the above gauges is reported in the Table 3.1 as mean absolute error (MAE) and phase shift (ΦE) at each tide gauge location.

Table 3.1: Model calibration results compared to synthesised water levels at tidal gauges

Location	MAE (m)	ΦE (min)
Gladstone Dock	0.20	-10
Port St Mary	0.11	0
Workington	0.11	0
Barmouth	0.12	-30
Holyhead	0.10	0
Trearddur Bay	0.15	-10

The MAE of the water level are below 5% of a mean spring tide range at all of these locations, which is considered excellent and provide confidence in the 2D model overall. Figure 3.7 through to Figure 3.12 below show, for the whole period, the predicted water levels traces compared to the tidal gauges.

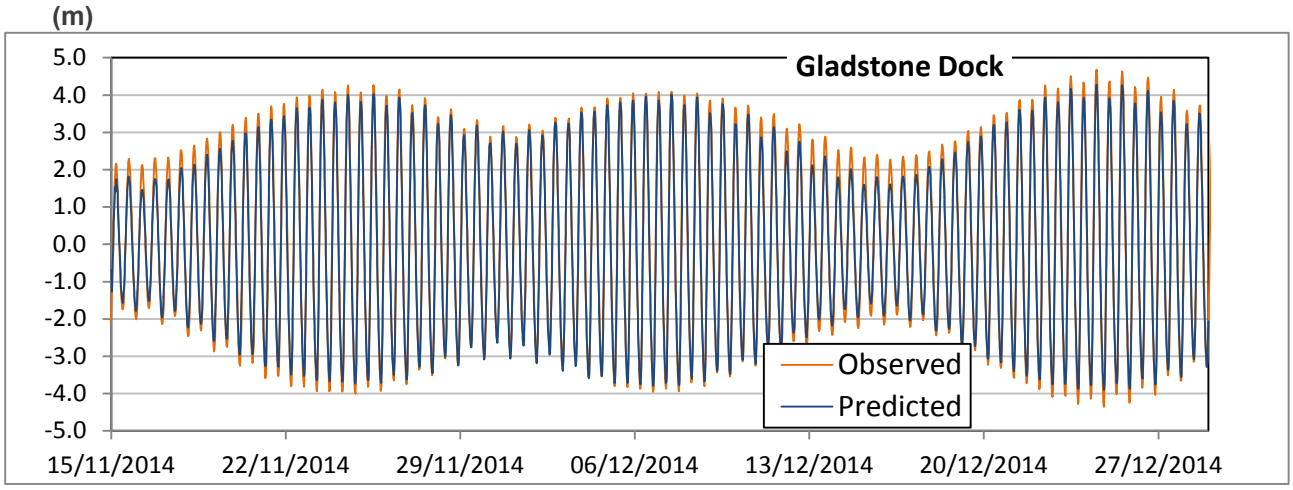

Figure 3.7: Overview comparison of model calibration results at Gladstone Dock

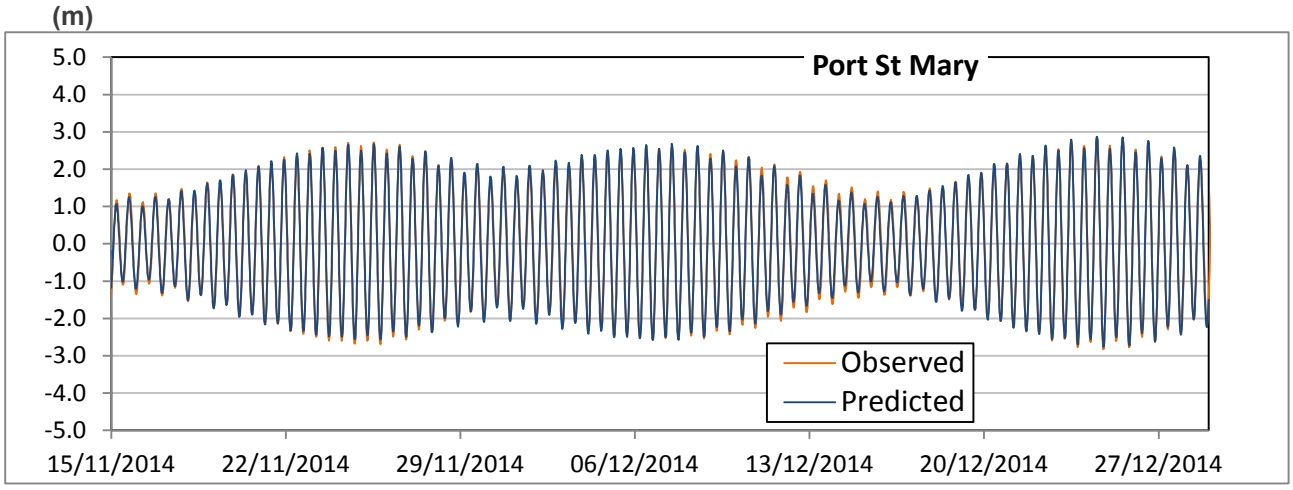

Figure 3.8: Overview comparison of model calibration results at Port St Mary

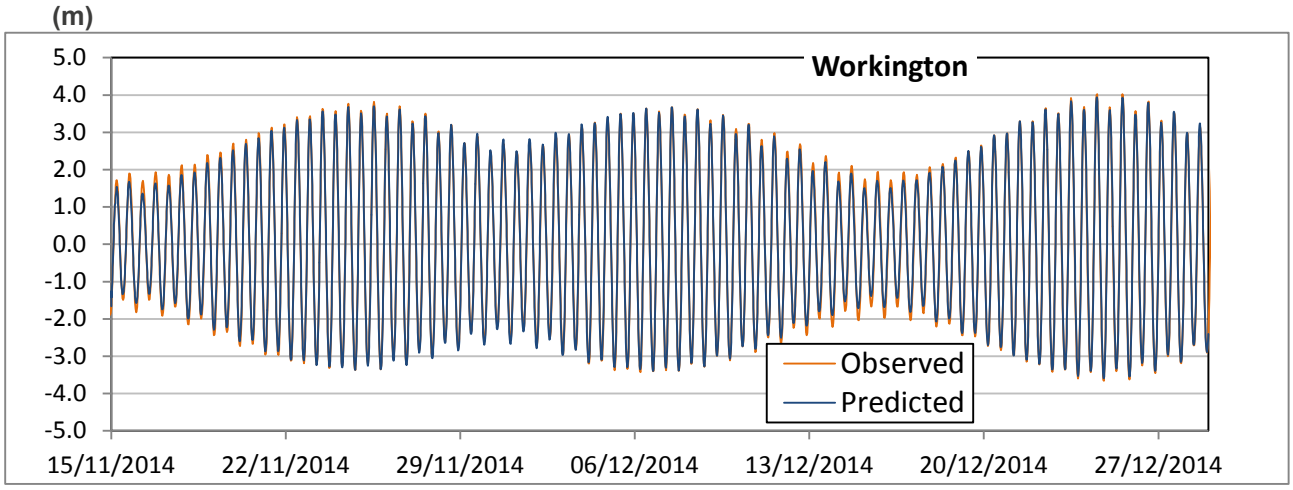

Figure 3.9: Overview comparison of model calibration results at Workington

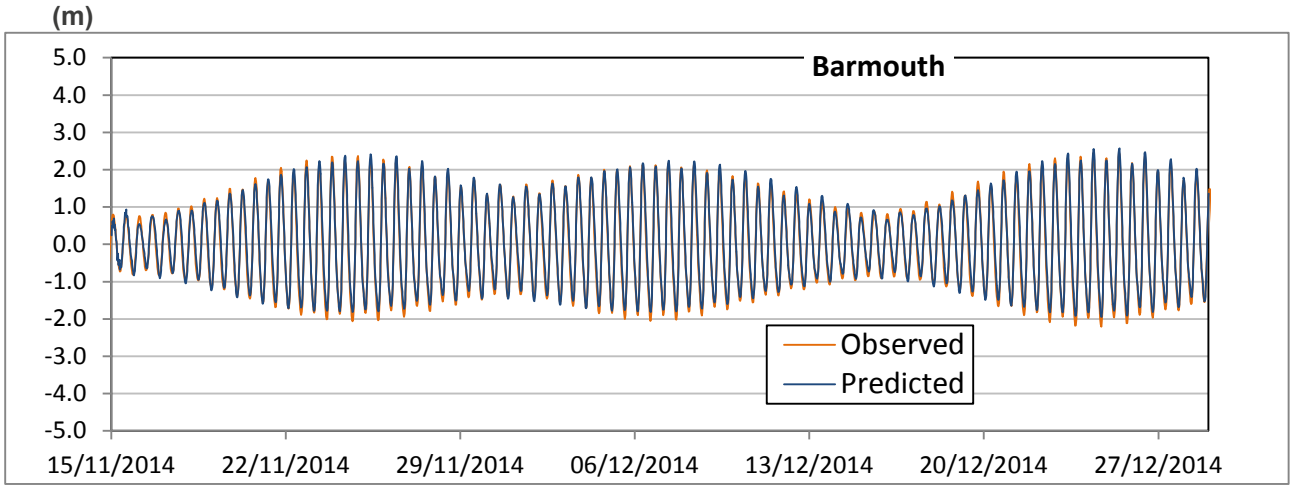

Figure 3.10: Overview comparison of model calibration results at Barmouth

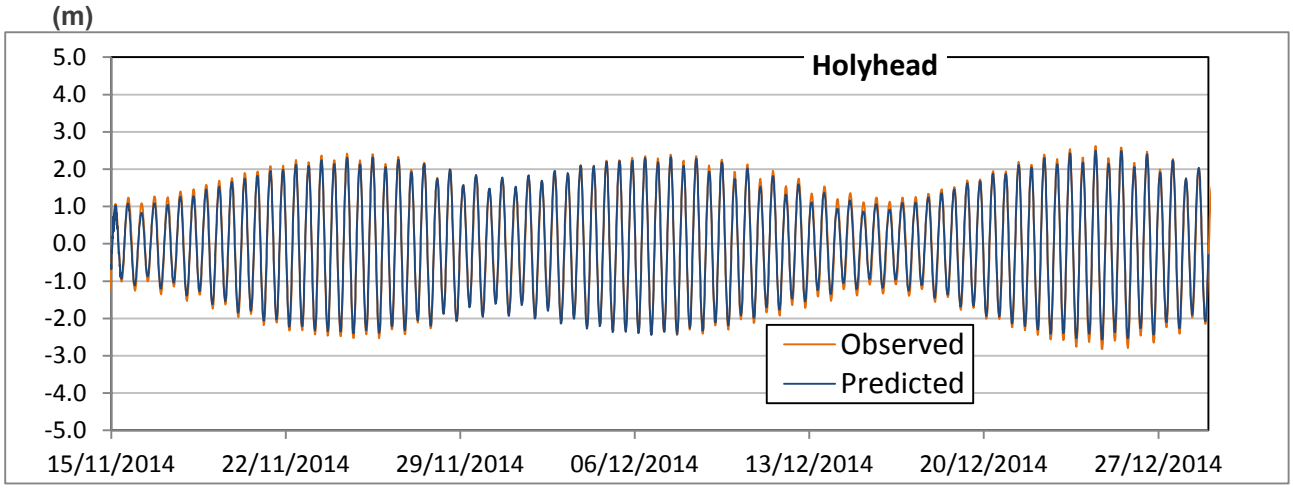

Figure 3.11: Overview comparison of model calibration results at Holyhead

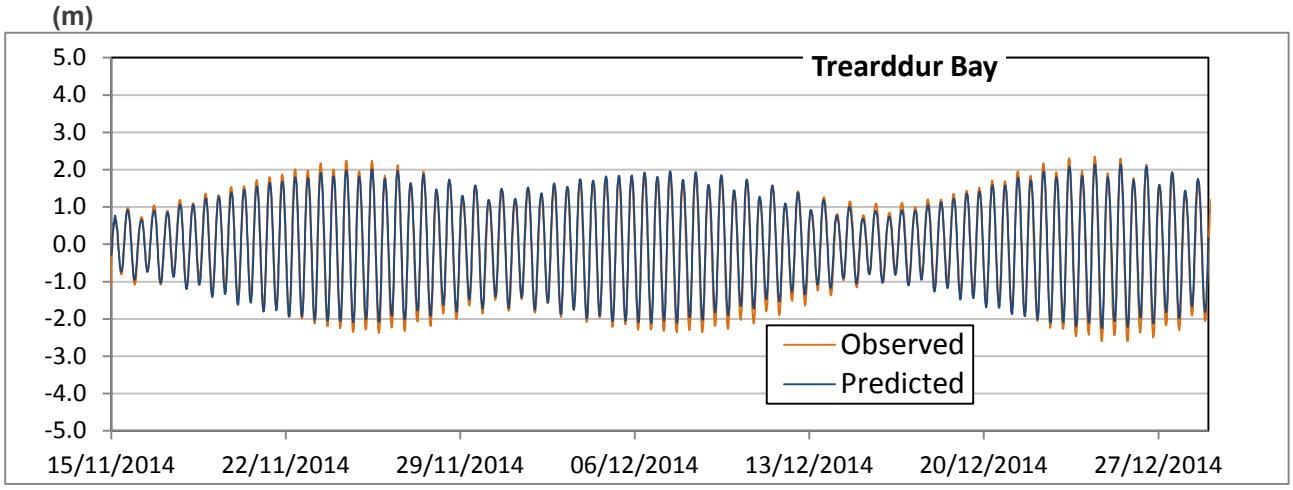

Figure 3.12: Overview comparison of model calibration results at Trearddur Bay

Similarly, Figure 3.13 through to Figure 3.18 highlight the same results for a shorter period of time.

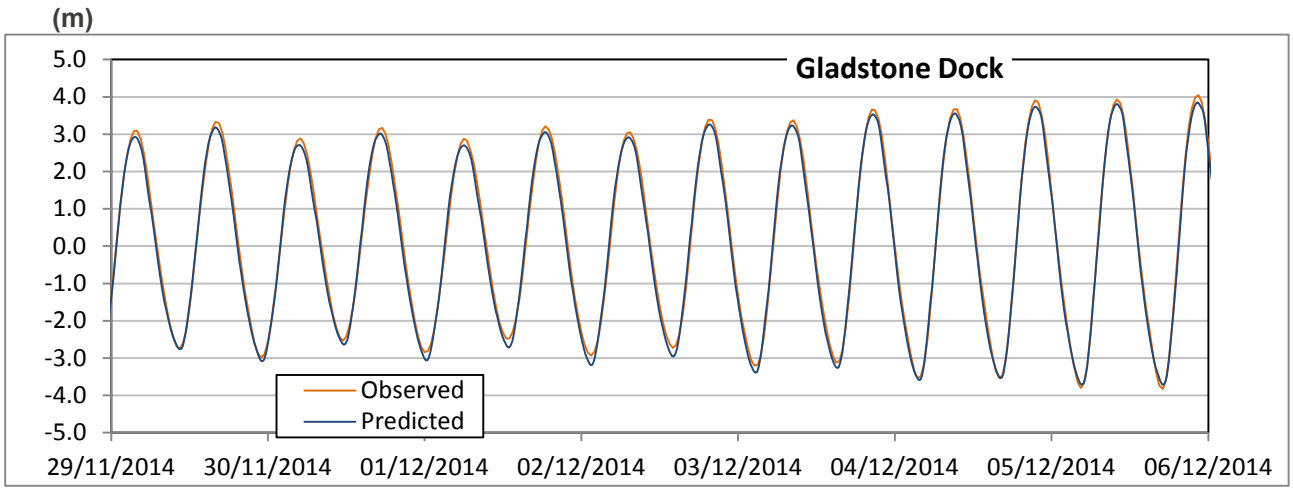

Figure 3.13: Highlighted comparison of model calibration results at Gladstone Dock

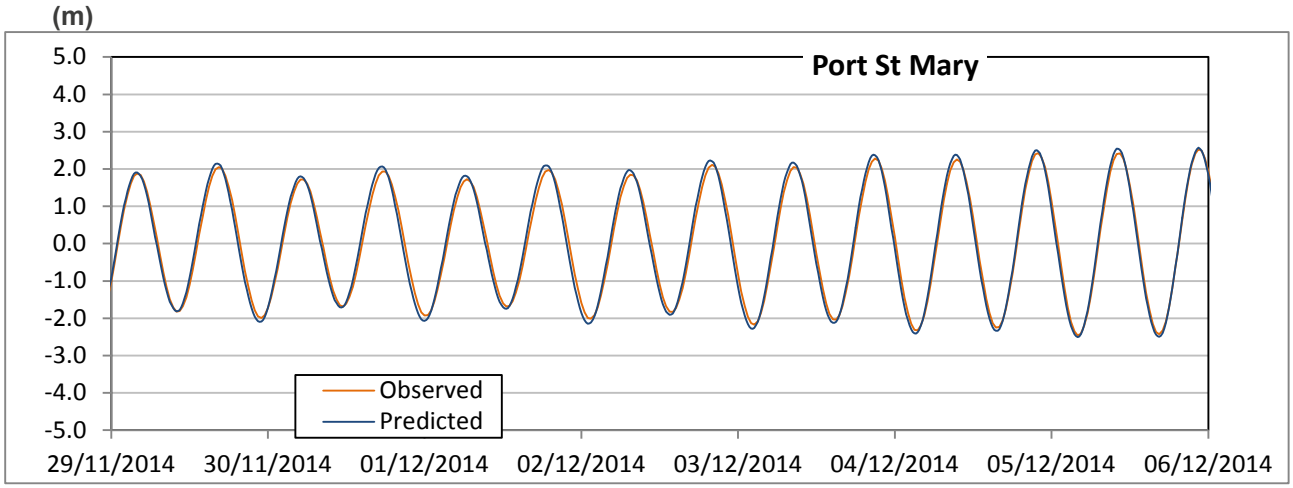

Figure 3.14: Highlighted comparison of model calibration results at Port St Mary

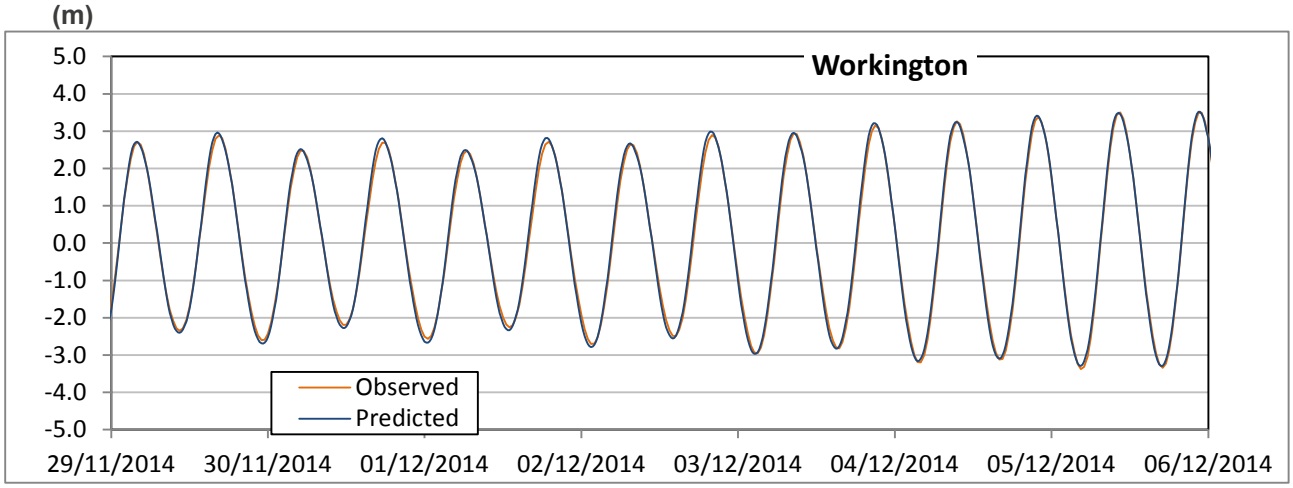

Figure 3.15: Highlighted comparison of model calibration results at Workington

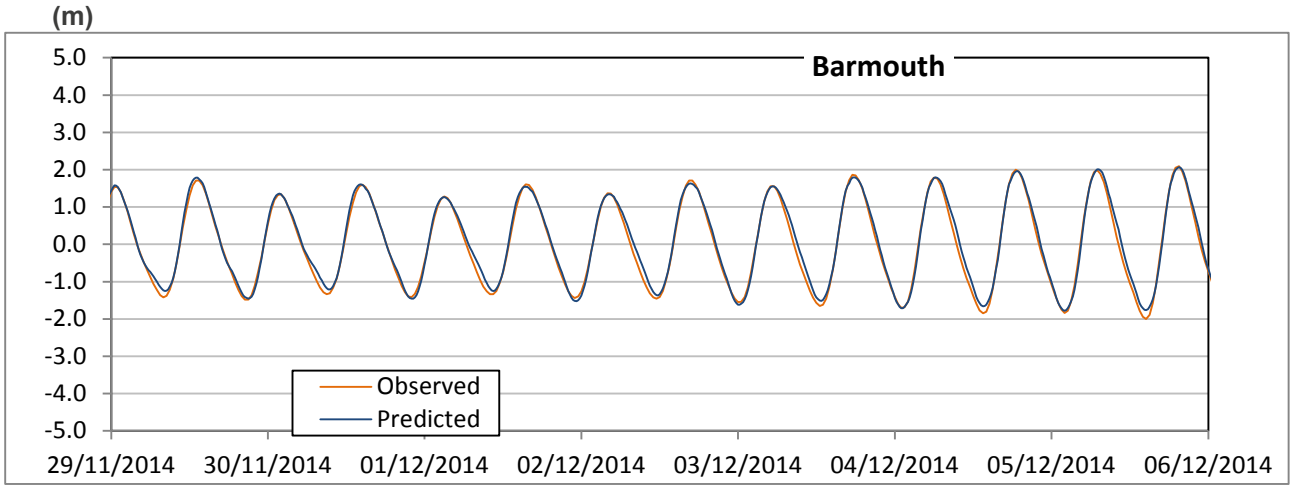

Figure 3.16: Highlighted comparison of model calibration results at Barmouth

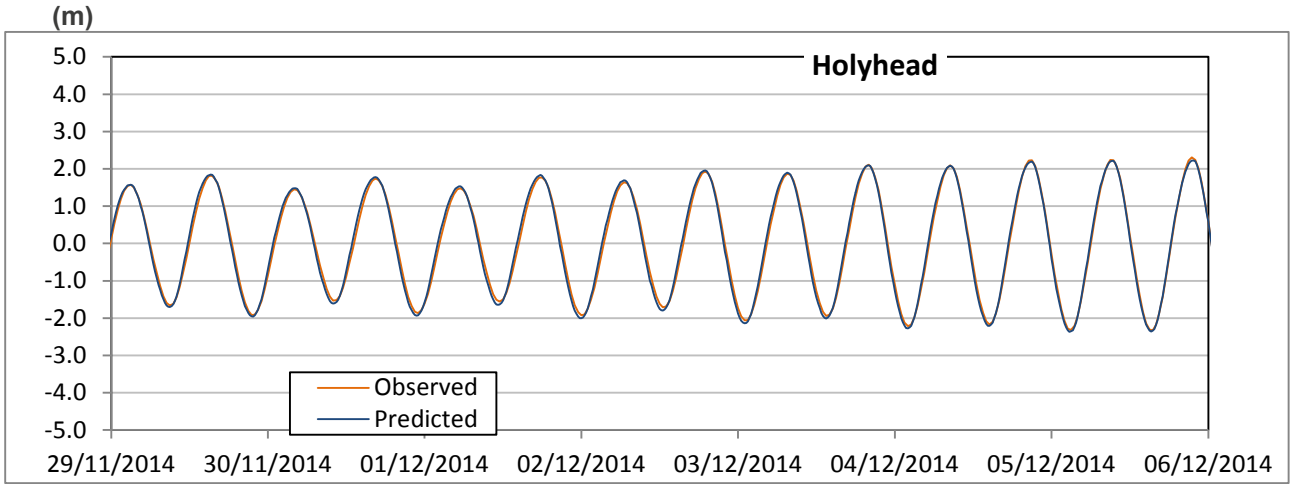

Figure 3.17: Highlighted comparison of model calibration results at Holyhead

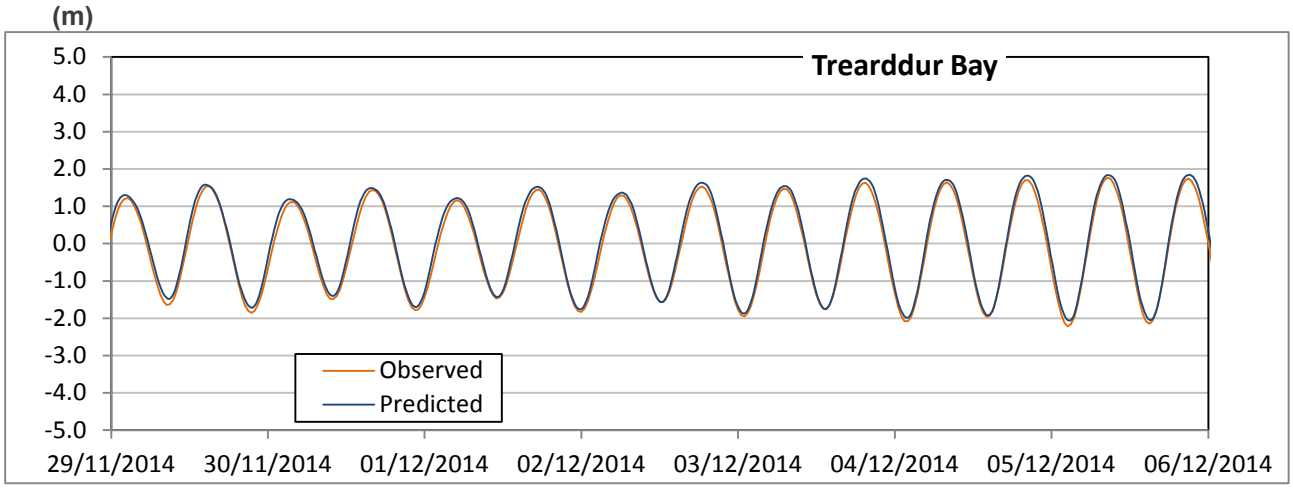

Figure 3.18: Highlighted comparison of model calibration results at Trearddur Bay

From the figure above, it can be seen that there is a very good comparison between model-based predicted water levels and record-based tidal gauge levels.

3.2.2. Model validation, water levels

As prescribed in the IEC TS 62600-201 guidelines, the model has been further validated against available local data from the two OpenHydro ADCP deployments. Having analysed the ADCP water depth information in terms of its tidal harmonics and re-synthesised the time history for the same period, a comparison with the 2D model is possible.

Similarly to the model calibration exercise (see Section 3.2.1), Figure 3.19 and Figure 3.20 show, for the whole period, the predicted water levels traces compared to their ADCP equivalent, at positions 1 and 2 respectively. In this analysis the predicted current patterns are shown in dark blue, the observed current patterns in orange.

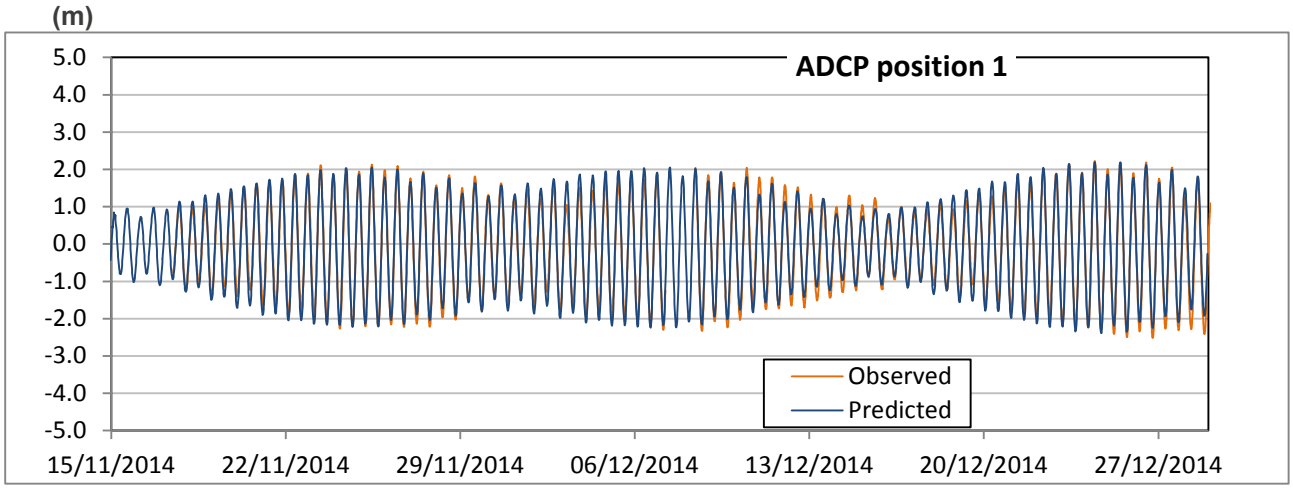

Figure 3.19: Overview comparison of model validation water depths at ADCP position 1

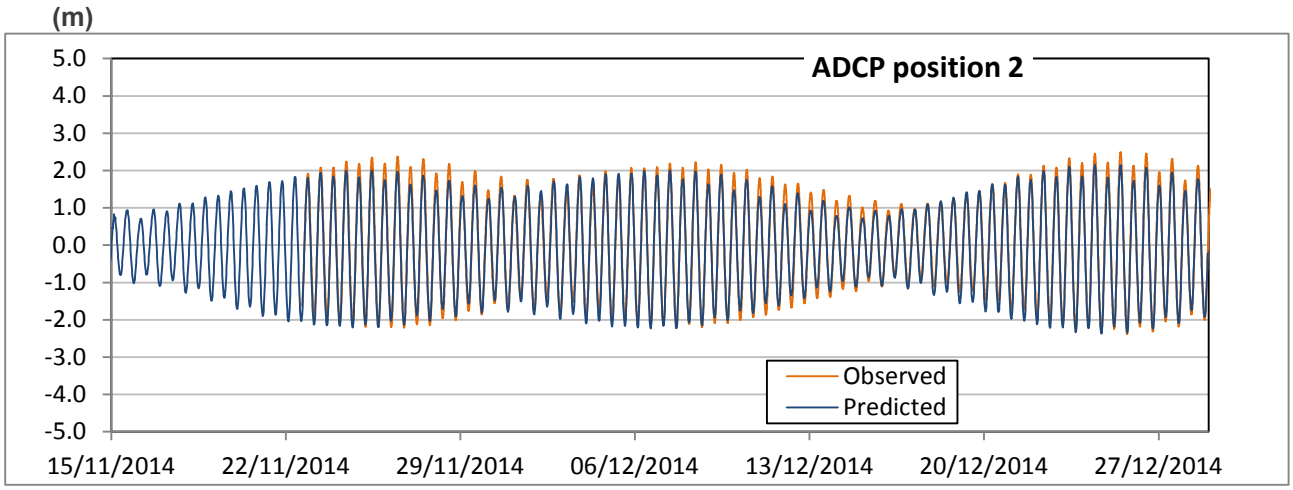

Figure 3.20: Overview comparison of model validation water depths at ADCP position 2

Figure 3.21 and Figure 3.22 highlight the same results for a shorter period of time.

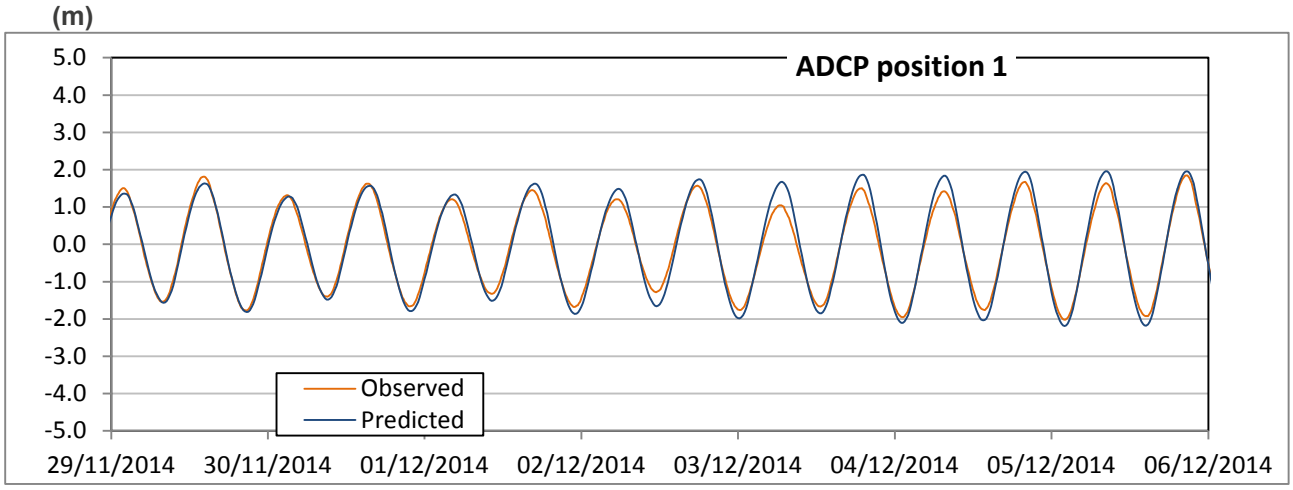

Figure 3.21: Highlighted comparison of model validation water depths at ADCP position 1

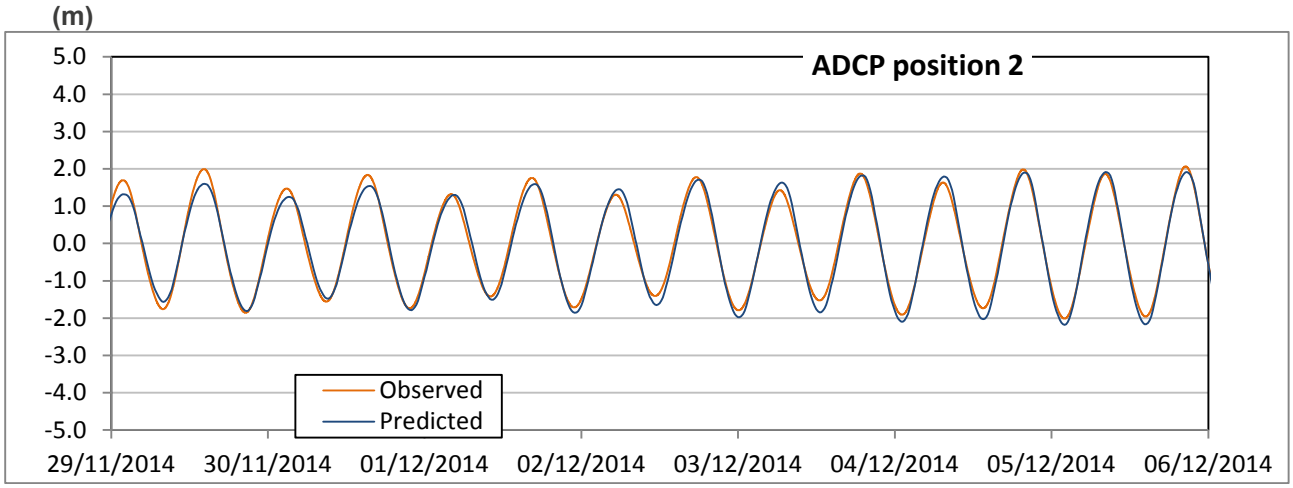

Figure 3.22: Highlighted comparison of model validation water depths at ADCP position 2

A comparison of the model results to the water levels re-synthesised at the ADCP positions is reported in the Table 3.2 as mean absolute error (MAE) and phase shift (ΦE).

Table 3.2: Model validation results compared to observed water levels at ADCP positions 1 and 2

Location	MAE (m)	ΦE (min)
ADCP position 1	0.15	-15
ADCP position 2	0.15	-15

Considering the uncertainties observed during the ADCP data review (see Section 2.2.3), these comparative results remain good, further validating the 2D model.

3.2.3. Model validation, current velocities

The model has been further validated against current velocities available from the two OpenHydro ADCP deployments. Again, having analysed the ADCP current velocity components in terms of their combined tidal harmonics and re-synthesised the time history for the same period, a comparison with the 2D model is possible.

The comparison of the 2D model with the measured current speed and direction is shown in the next four figures, for positions 1 and 2, as an overview over the whole period. Again, the predicted current patterns are shown in dark blue, the observed current patterns in orange.

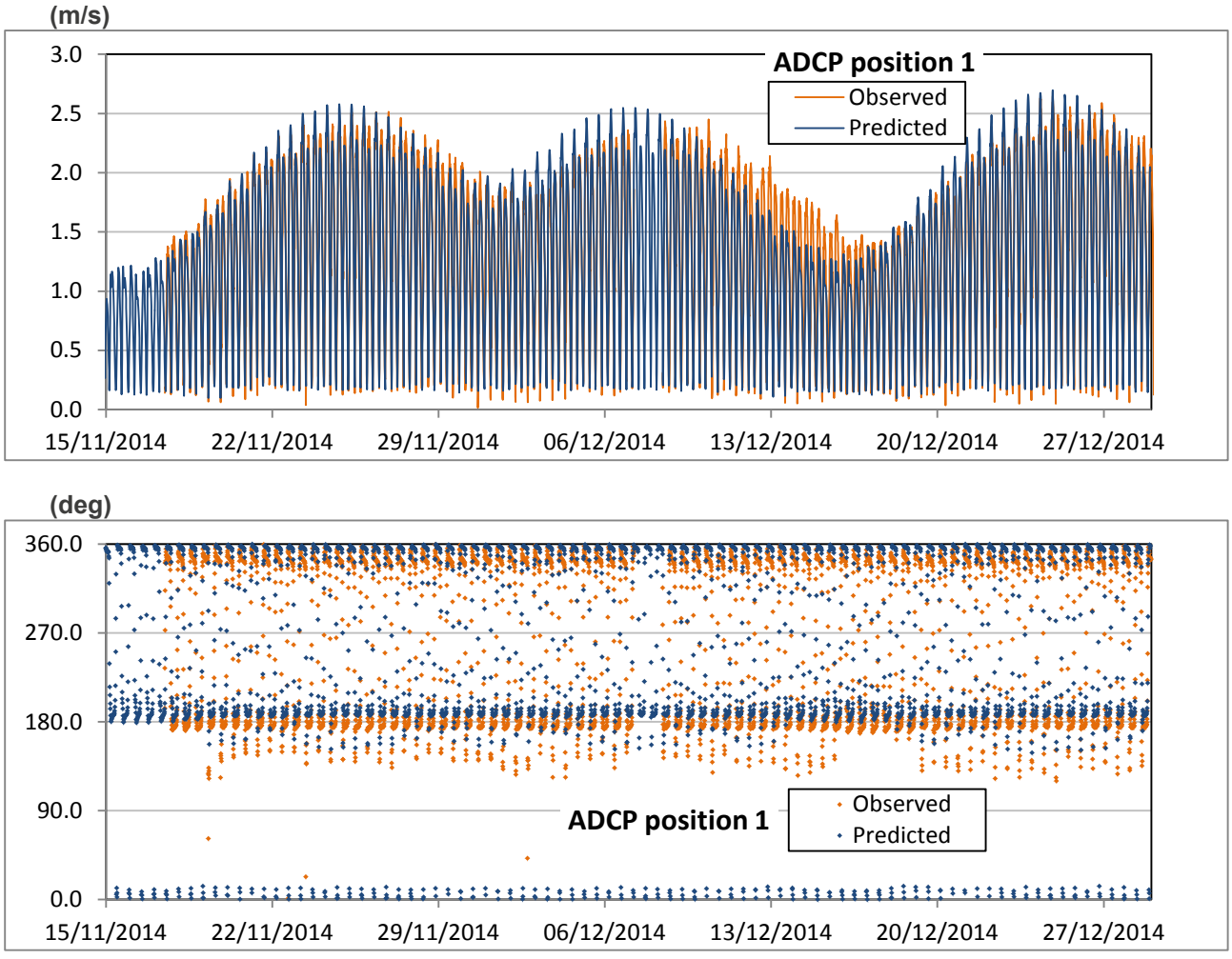

Figure 3.23: Overview comparison of model validation current speeds and directions at ADCP position 1

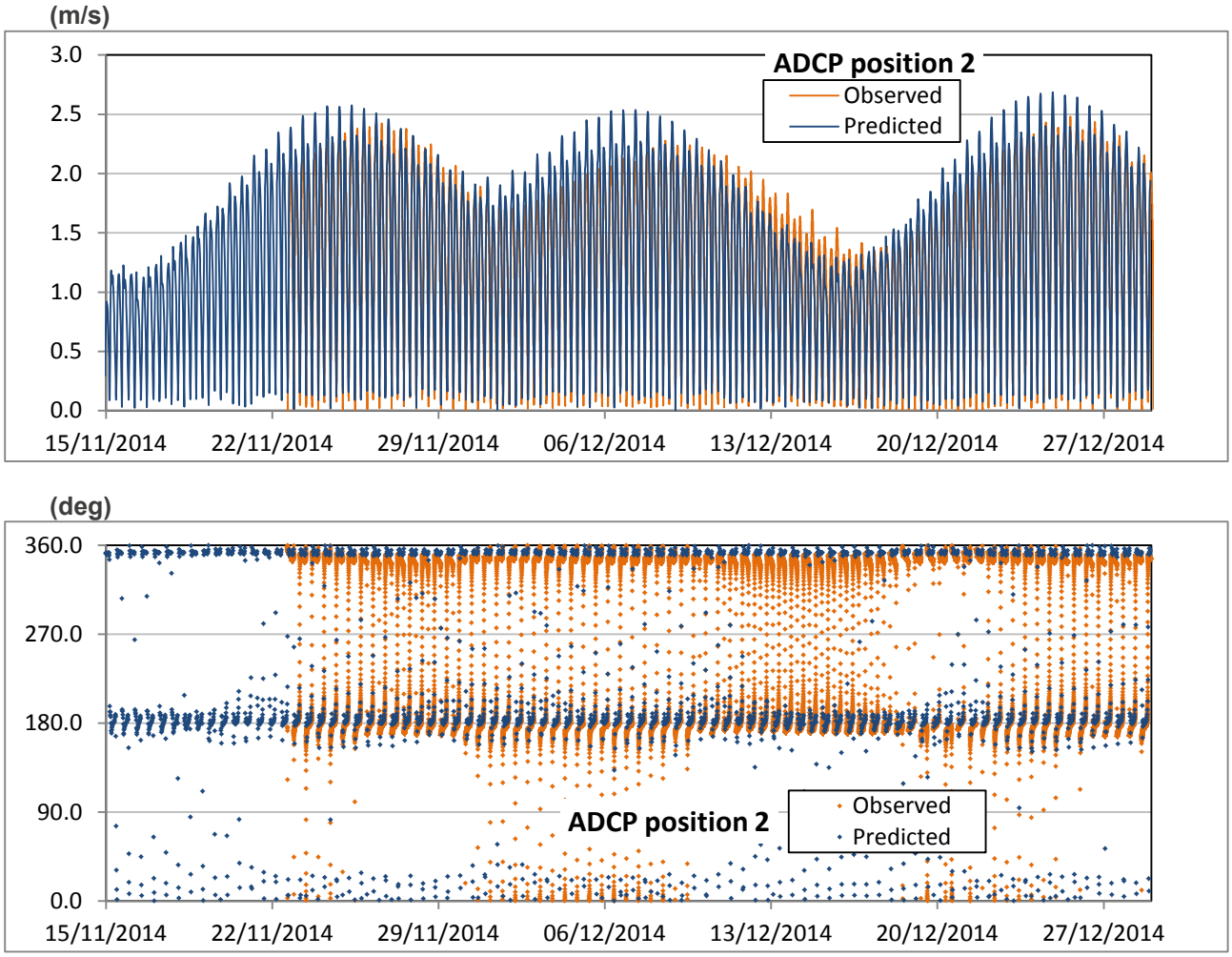

Figure 3.24: Overview comparison of model validation current speeds and directions at ADCP position 2

The mean absolute error (MAE) on current speed, tidal phase shift (ΦE), and current direction are reported in Table 3.3 below.

Table 3.3: Model validation results compared to observed data at ADCP positions 1 and 2

Location	MAE (m/s)	ΦE (min)	MAE (deg)
ADCP position 1	0.16	-5	20
ADCP position 2	0.16	-5	16

Considering the uncertainties observed during the ADCP data review (a data gap at position 1 and a non-functioning pressure gauge at position 2, see Section 2.2.3), these comparative results are good, with a MAE about 6% of the peak current measured, sufficiently close to the approximately 5% (“c. 5%”) recommended by the IEC TS 62600-201 guidelines, and significantly better than the more typical 10% criterion, beyond which an explanation should be provided as to why the result is less accurate.

3.2.4. Further model verification

Other types of analysis can be carried out to compare ADCP current velocities with model predictions. Two are presented here.

The first analysis is to create distributions of current speeds for the entire validation period, sorting speed values in bins (say 0.1 m/s in size). For consistency within this report, the predicted distribution is dark blue and the observed distribution is orange. Figure 3.25 relates to ADCP position 1; Figure 3.26 relates to ADCP position 2.

The analysis shows a good correspondence between predicted and observed, including in the ranges of the current speeds contributing most to the maximum power available (above 2.0 m/s), with the model results slightly higher at position 2 and slightly lower at position 1.

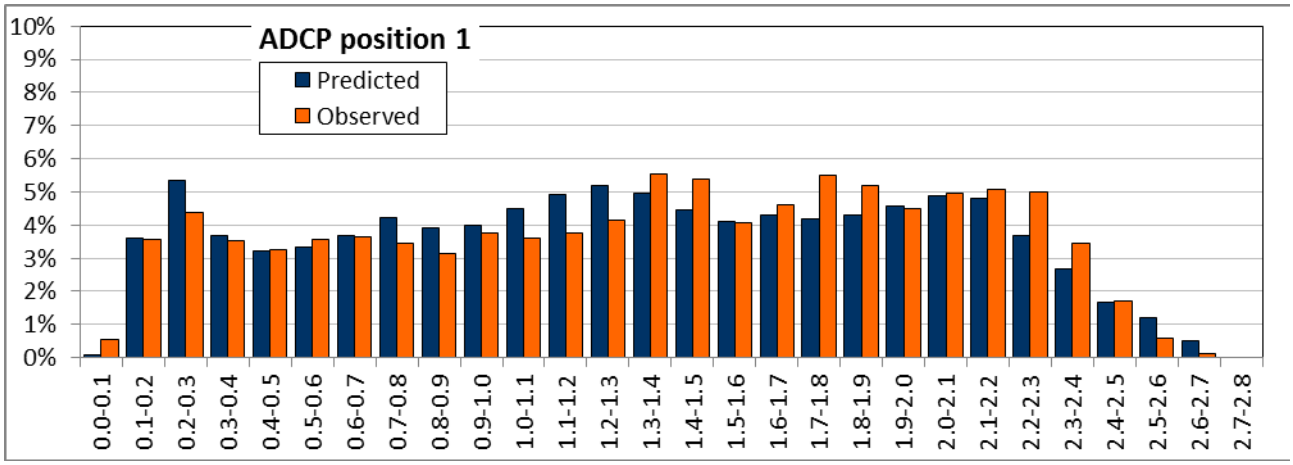

Figure 3.25: Model predicted and observed distribution of current speeds (m/s) at ADCP position 1

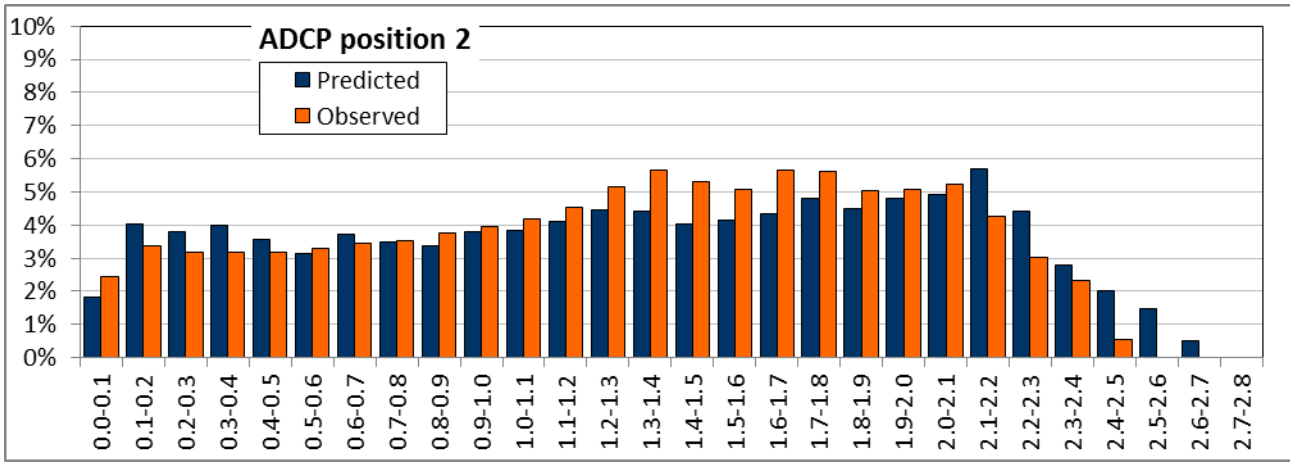

Figure 3.26: Model predicted and observed distribution of current speeds (m/s) at ADCP position 2

The second analysis is to consider current tidal ellipses for the entire validation period. A tidal ellipse is a visual representation of the direction and strength of the flow throughout one or more tidal cycles and gives a

good indication of the major current axis. The rings on the ellipse represent the current speed. Each point represents a time step in the model or an observation in the record. In this analysis the predicted current patterns are shown in dark blue, the observed current patterns in orange. Figure 3.27 relates to ADCP position 1; Figure 3.28 relates to ADCP position 2.

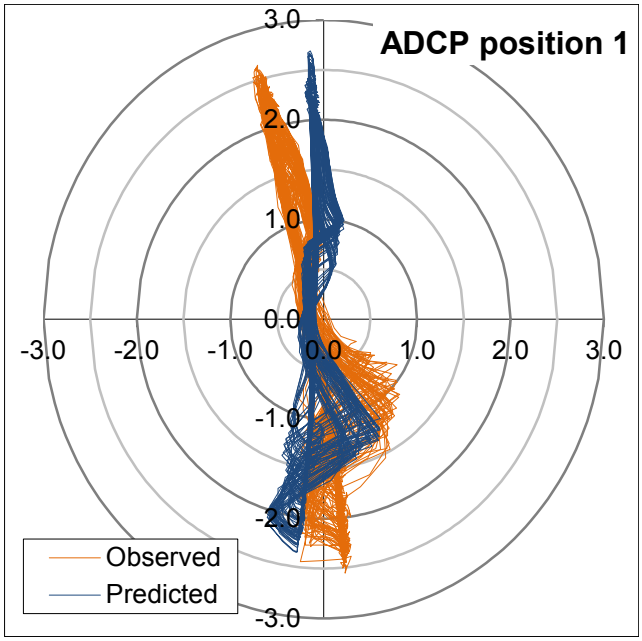

Figure 3.27: Predicted and observed tidal ellipse at ADCP position 1

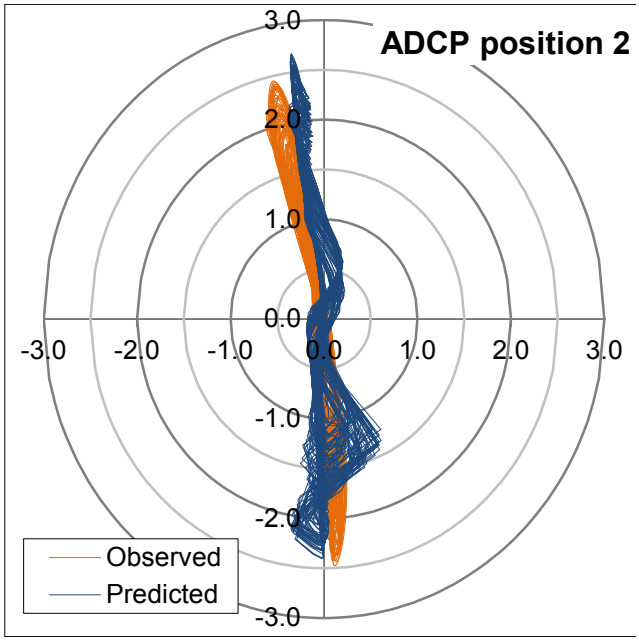

Figure 3.28: Predicted and observed tidal ellipse at ADCP position 2

These show that the variability in current direction is higher when currents are towards the south than to the north.

3.3. Model setup conclusion

As concluded during the data review (see Section 2.2.3) there are some deficiencies in the raw ADCP data resulting in a non-optimum synthetisation of tidal water levels and current velocities. However, the comparative figures and error measures for the two ADCP positions are encouraging. The period of time when the velocity are within certain speed bin (looking at the distributions) seems balanced over the two ADCP positions.

The 2D model setup is considered very good for the purpose of the project.

4. Tidal stream turbines

The validated model was used to study the impact of including the operating turbines, operating in accordance with the generic turbine characteristics, dimensions, and power and thrust curves supplied by Menter Môn.

Four scenarios were considered (with 102, 204, 306 and 408 turbines), in addition to a baseline scenario (without any turbines). A final set of turbine characteristics was generated through an iterative process with Menter Môn, varying combinations of power and thrust curves.

It is understood that the objective of this project has not been to consider optimisation of turbine placements within the MDZ.

4.1. Turbine characteristics

Owing to the uncertainty with respect to which turbines are being deployed at different locations within the MDZ, a generic turbine rotor has been used in all simulations. After initial investigations with 15m rotor diameter (D) turbines at 6D spacing (east to west), the generic turbines adopted for this study were 20m rotor diameter at 4.5D spacing (east to west). The assumed turbine characteristics are given in Table 4.1 below, with assumed thrust and power curves provided in Figure 4.1 and Figure 4.2 respectively.

In view of the generic turbine being used, and other uncertainties in the modelled flow speeds, the upstream free stream depth averaged velocity was used directly to drive the turbines. Desk based calculations show that for scenario 3 and the assumptions here (axis 15m off the seabed, and turbine diameter of 20m), there could be a further 2% increase in velocity, and hence 6% increase in power over the reported values. This will depend on the final specific designs adopted.

Table 4.1: Generic Turbine Characteristics

Characteristic	Assumed Value
Rotor diameter (D)	20m
Rated flow speed	2.015 m/s
Cut-in flow speed	0.8 m/s
Rated mechanical (electrical) power	659kW (595kW)
Power Curve	Variable with flow speed
Thrust Curve	Variable with flow speed
Position in water column	Mid depth

Source: Menter Môn

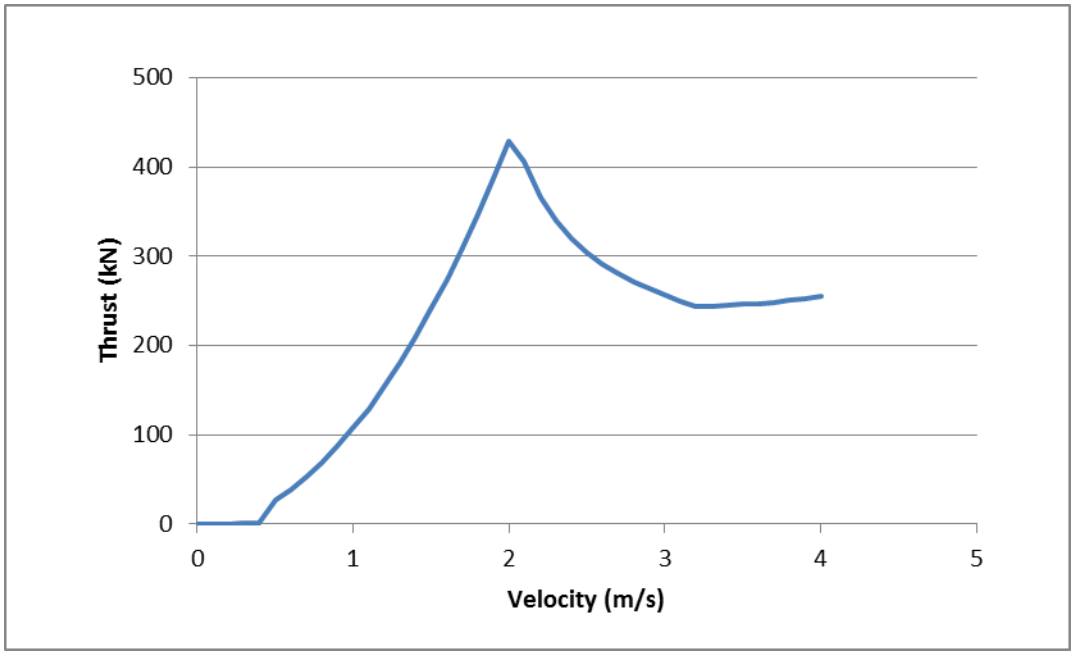

Figure 4.1: Thrust curve for generic turbine (Menter Môn)

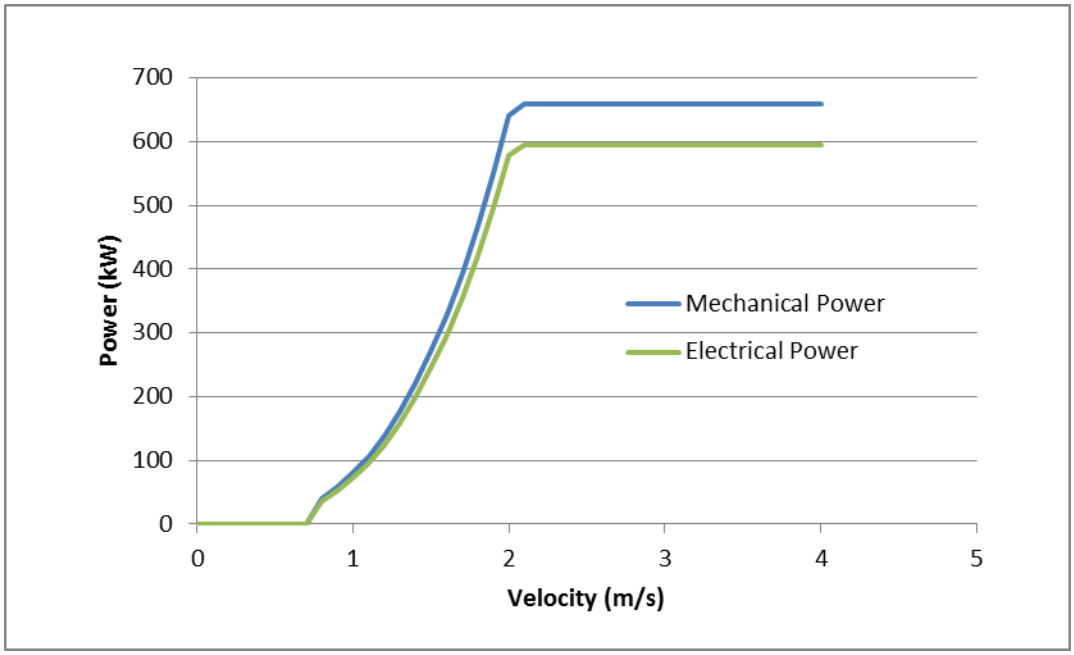

Figure 4.2: Power curve for generic turbine. Note that electrical power was derived by applying a factor of 0.903 to the mechanical power (Menter Môn)[1]

1 Calculated on the basis of 0.95 (mechanical), 0.97 (generation), 0.98 (transmission), total = 0.903

4.2. Turbine locations

The installation of the turbines into the model was discussed with Menter Môn and it was determined that the following rules should apply:

- The first turbine should be installed in the centre (north-south) of the respective Sub-Zone;
- Turbines should be evenly spaced (by 4.5D) moving westwards along the line;
- Successive rows should be added, as required, spaced 333m from the first row and with the turbines staggered (by 2.25D) in a west-east direction between rows.

The turbine arrangements are shown in Figure 4.3 below.

The number of turbines and rated capacity installed for each scenario is provided in Table 4.2 below.

The generic turbine characteristics and installation pattern were selected to provide a reasonable first estimate of the interactions between zones, without seeking to pre-empt the design process. Interactions for different arrays of turbines, for instance in blocks nearer the coast (but within a subzone), would require further assessment.

Table 4.2: Number of turbines and rated capacity distribution (Electrical Power, MW) in each scenario and Sub-Zone

	Scenario 1 No. of turbines	Rated power (MW)	Scenario 2 No. of turbines	Rated power (MW)	Scenario 3 No. of turbines	Rated power (MW)	Scenario 4 No. of turbines	Rated power (MW)
1	0	0	0	0	0	0	51	30.345
2	17	10.115	34	20.23	51	30.345	51	30.345
3	17	10.115	34	20.23	51	30.345	51	30.345
4	17	10.115	34	20.23	51	30.345	51	30.345
5	17	10.115	34	20.23	51	30.345	51	30.345
6	17	10.115	34	20.23	51	30.345	51	30.345
7	0	0	0	0	0	0	51	30.345
8	17	10.115	34	20.23	51	30.345	51	30.345
Total	102	60.69	204	121.38	306	182.07	408	242.76

Source: Menter Môn. Note that in this report Sub-Zones 1-7 represent the north-south arranged adjacent east-west rectangular shaped Sub-Zones. Sub-Zone 8 represents the north-south aligned single Sub-Zone to the west.

Scenario 1

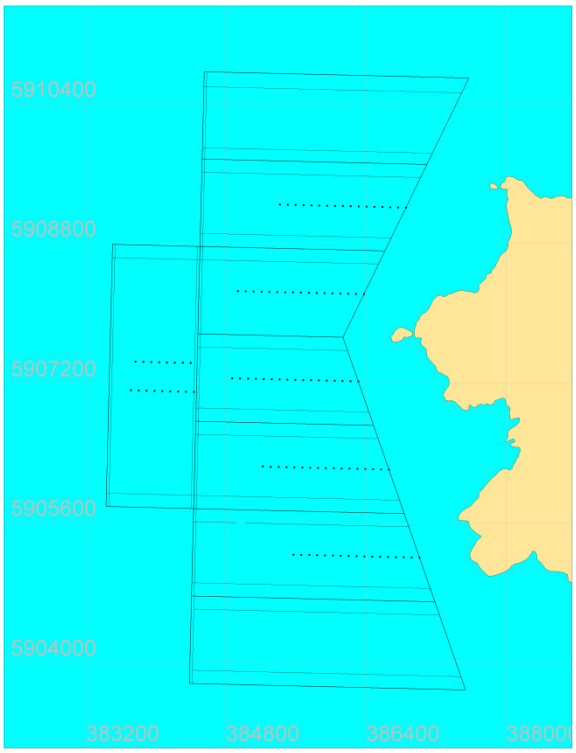

Scenario 2

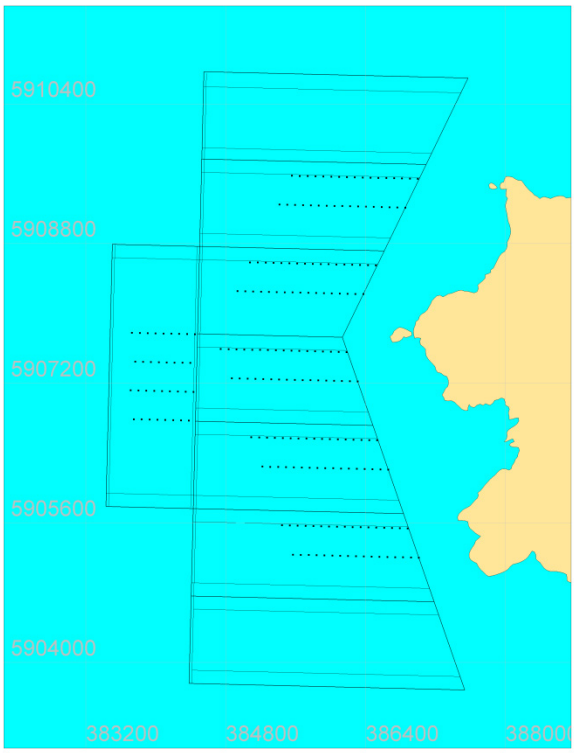

Scenario 3

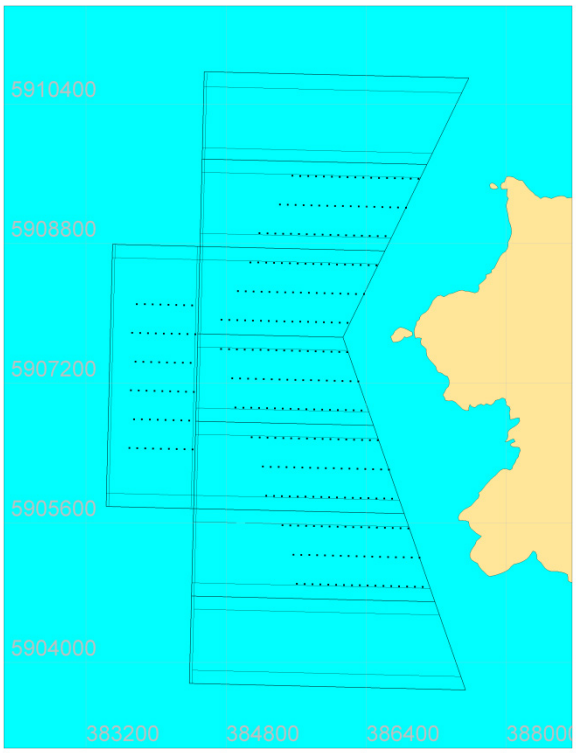

Scenario 4

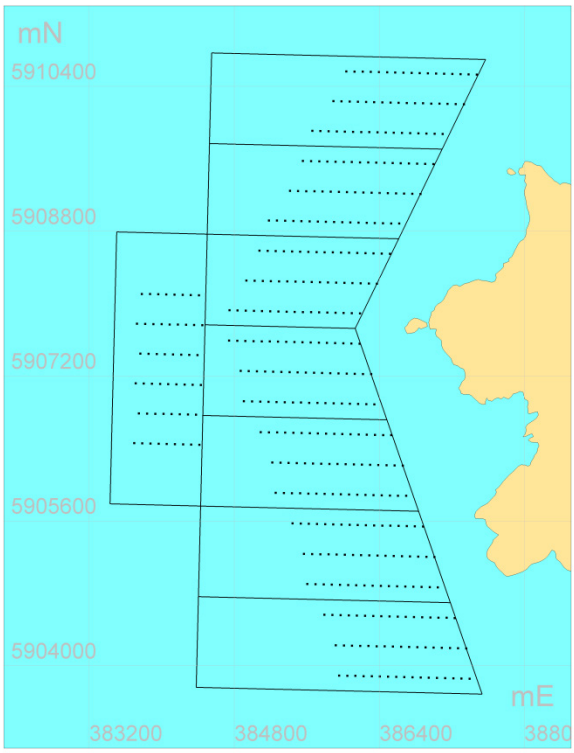

Figure 4.3: Turbine installation arrangements in the model

Source: Menter Môn

5. Model simulations

Five scenarios were simulated using the model. These cover the "no turbines" case plus each of the four turbine scenarios:

- Baseline No turbines installed;
- Scenario 1 60 MW installed;
- Scenario 2 120 MW installed;
- Scenario 3 approximately 180 MW installed;
- Scenario 4 approximately 240 MW installed.

The Baseline case was run using both the Scenario 1 to 3 model mesh and the Scenario 4 model mesh (see Section 3.1.1). This ensures that the assessment of the effect of introducing turbines is not influenced by changes in the mesh between Baseline and each of the with-turbines scenarios.

For each model run (using a complete lunar cycle), outputs were provided at a series of measurement points (at 100m intervals) along the boundaries of the buffer zones. Outputs include mean velocity, peak velocity, mean spring peak velocity and average power density.

5.1. Modelled power extraction

The model was run for the same 44 day period as for the model validation and the results analysed for a full lunar month (29.5 days). The full model results showing simulated (electrical) power extraction are shown in Figure 5.1 to Figure 5.4 below.

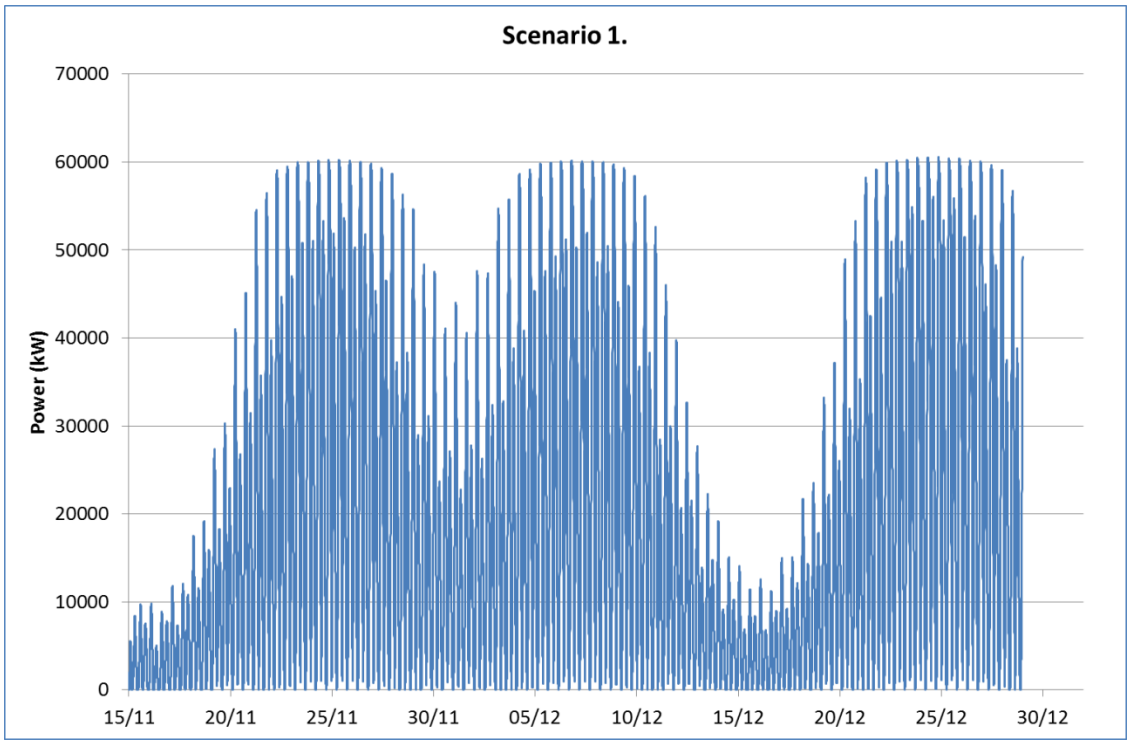

Figure 5.1: Modelled electrical power extraction (Scenario 1)

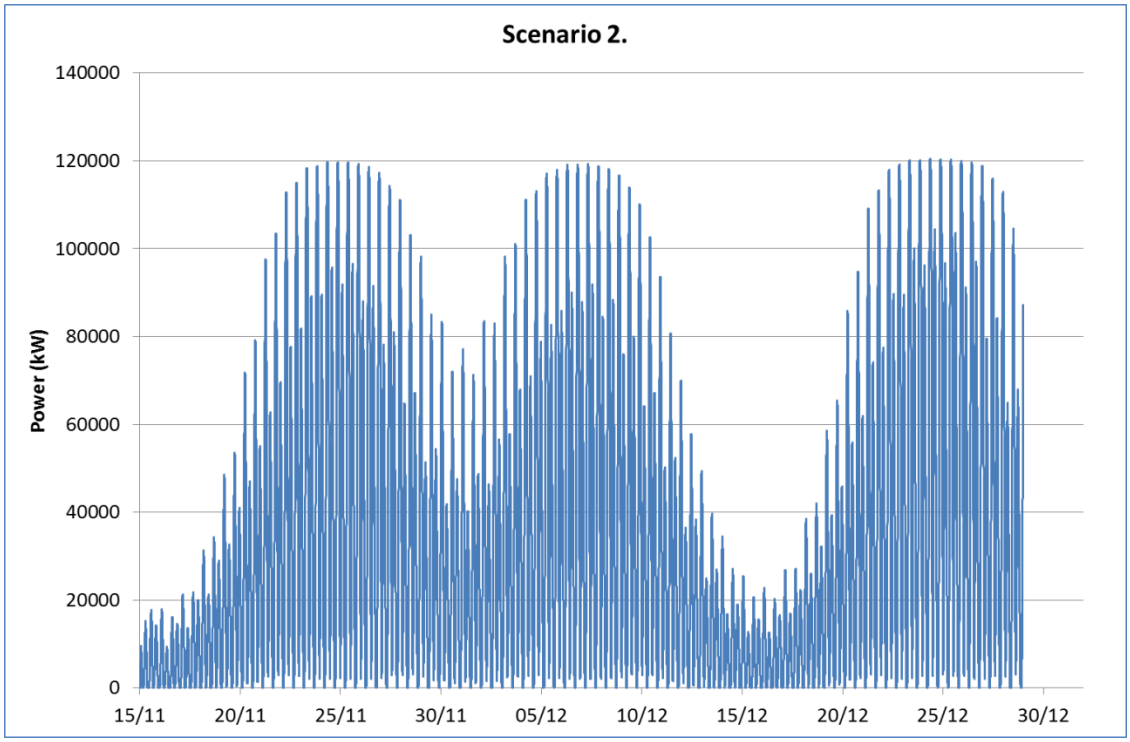

Figure 5.2: Modelled electrical power extraction (Scenario 2)

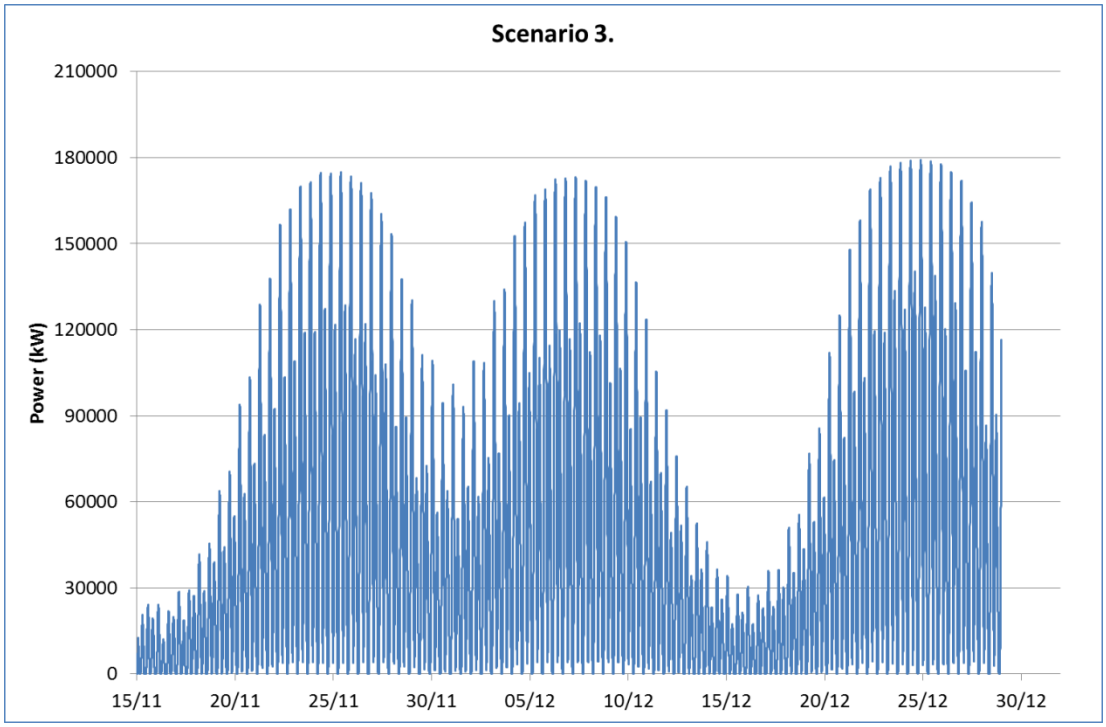

Figure 5.3: Modelled electrical power extraction (Scenario 3)

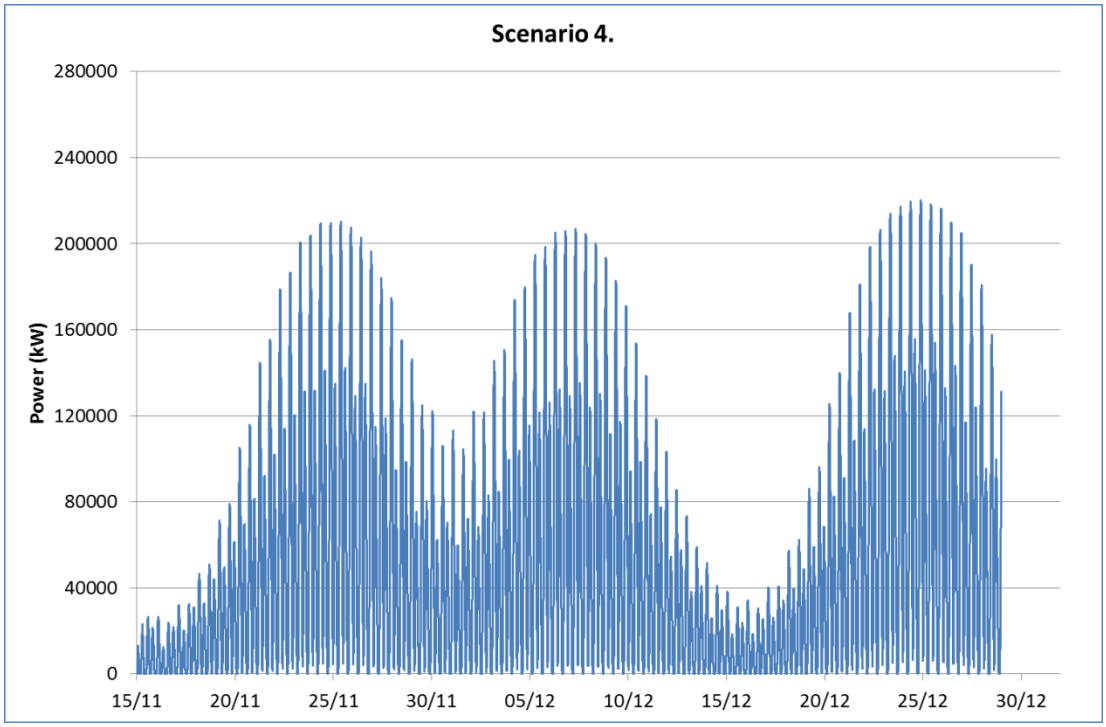

Figure 5.4: Modelled electrical power extraction (Scenario 4)

5.1.1. Discussion of modelled power extraction

Figure 5.1 to Figure 5.3 above show the full simulated power at one minute intervals for a total duration of 44 days, corresponding to the calibration period and allowing for model spin up time. The figures show the modelled power through three spring-neap cycles, starting on neap tides and showing three broad “peaks” corresponding to spring tide periods.

For a date of stated mean spring tide range (4.9m) at Holyhead, the model predicts the following peak total power for each scenario:

- Scenario 1 60 MW
- Scenario 2 120 MW
- Scenario 3 175 MW
- Scenario 4 209 MW.

For neap tides, the peak total power for each scenario is considerably less, reflecting the significantly lower tidal current speeds during neap tides.

Average power extraction

In accordance with IEC TS 62600-201:2015 recommendations it is also worth considering the average power over a lunar month and extrapolating through to a 19 year (nodal tidal cycle) long term average. The model computed the power produced by the array (with electrical conversion efficiency multiplier) for a 29.5 day simulation period (after model spin-up).

To extrapolate to a long period (19 years) we considered a single turbine at ADCP position 2. The table of power values as a function of current speed was used to compute a single turbine’s power output at this

location for a 19 year period using a tidal synthesis of the currents at this location including the modelled period. The power produced on average for the 29.5 day and 19 year period (in MW) were obtained and the ratio of these values was then used to extrapolate the whole array production for the modelled period to the longer period. This method avoids the need for a very long continuous model simulation.

Position 2 was used, as a better tidal analysis was produced here. The ratio to extrapolate from the 29.5 days period to the 19 year period was 0.937 (the modelled period had a slightly greater than average energy production). Results are summarised in Table 5.1 below.

Table 5.1: Average total power for model simulated lunar month and long term average

	Scenario 1 (MW)	Scenario 2 (MW)	Scenario 3 (MW)	Scenario 4 (MW)
Average power over simulated 29.5 day period	19	34	45	51
Estimated average power for 19 year period	18	32	43	48

Source: HR Wallingford

5.2. Modelled changes to peak flow speeds (spring tide)

The following series of figures shows the effects of the operating turbines on peak flows during a mean spring tide at Holyhead.

5.2.1. Baseline (no turbines)

Figure 5.5 below shows the peak depth averaged flow speeds for a mean spring tide range at Holyhead. Peak speeds are generally predicted to be faster through the eastern parts of the subzones, reaching in excess of 2.6-2.8m/s in most areas apart from the northernmost and southernmost subzones. The highest predicted flows speeds reach 4.0m/s just off Holy Island (shown by the small red area in the third most northerly subzone in Figure 5.5). For the western parts of the subzones, peak speeds are somewhat lower, reaching in excess of 2.2-2.6m/s. Figure 5.6 shows the 29.5 day mean flow speed for this scenario.

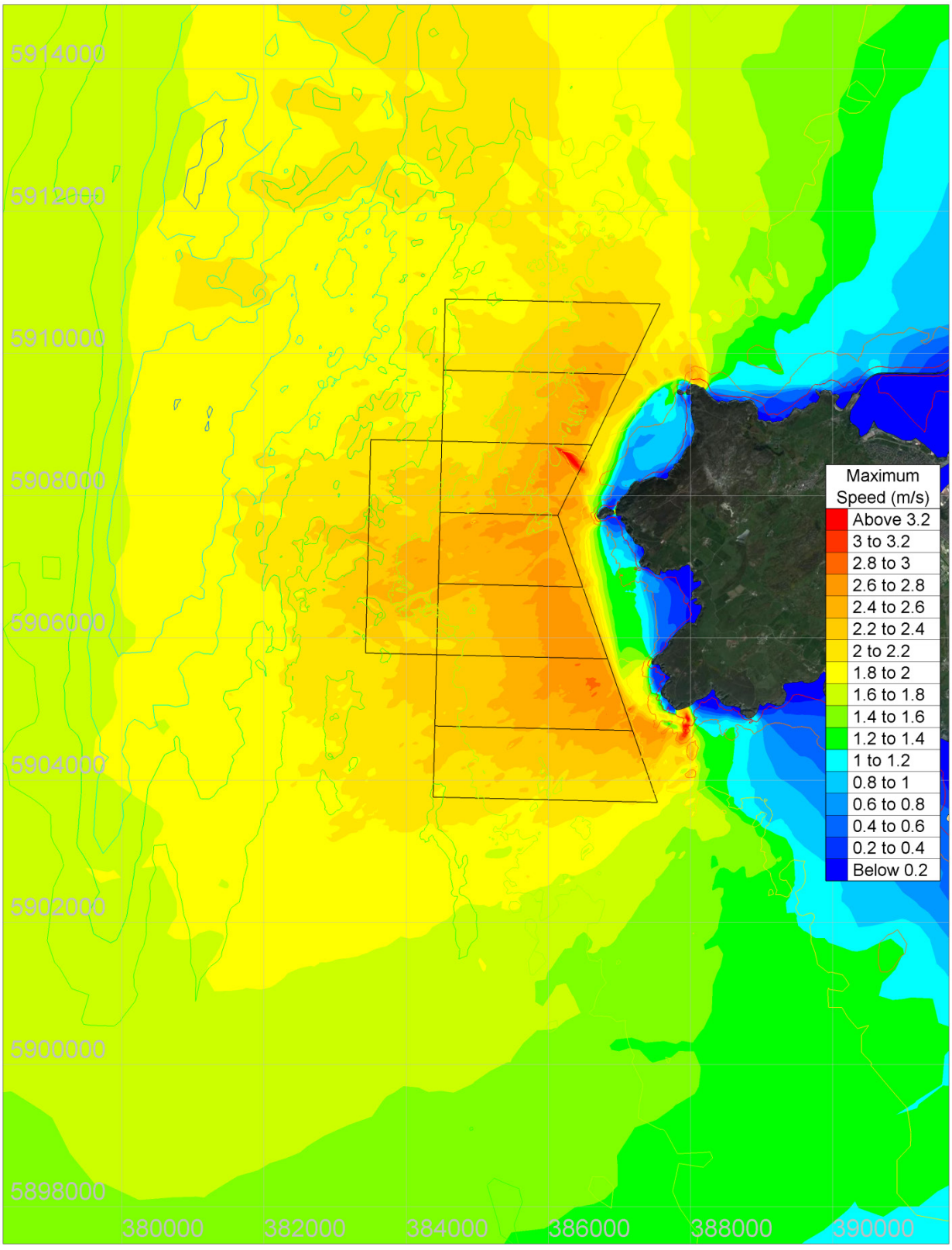

Figure 5.5: Baseline peak flow speed (m/s) for mean spring tide

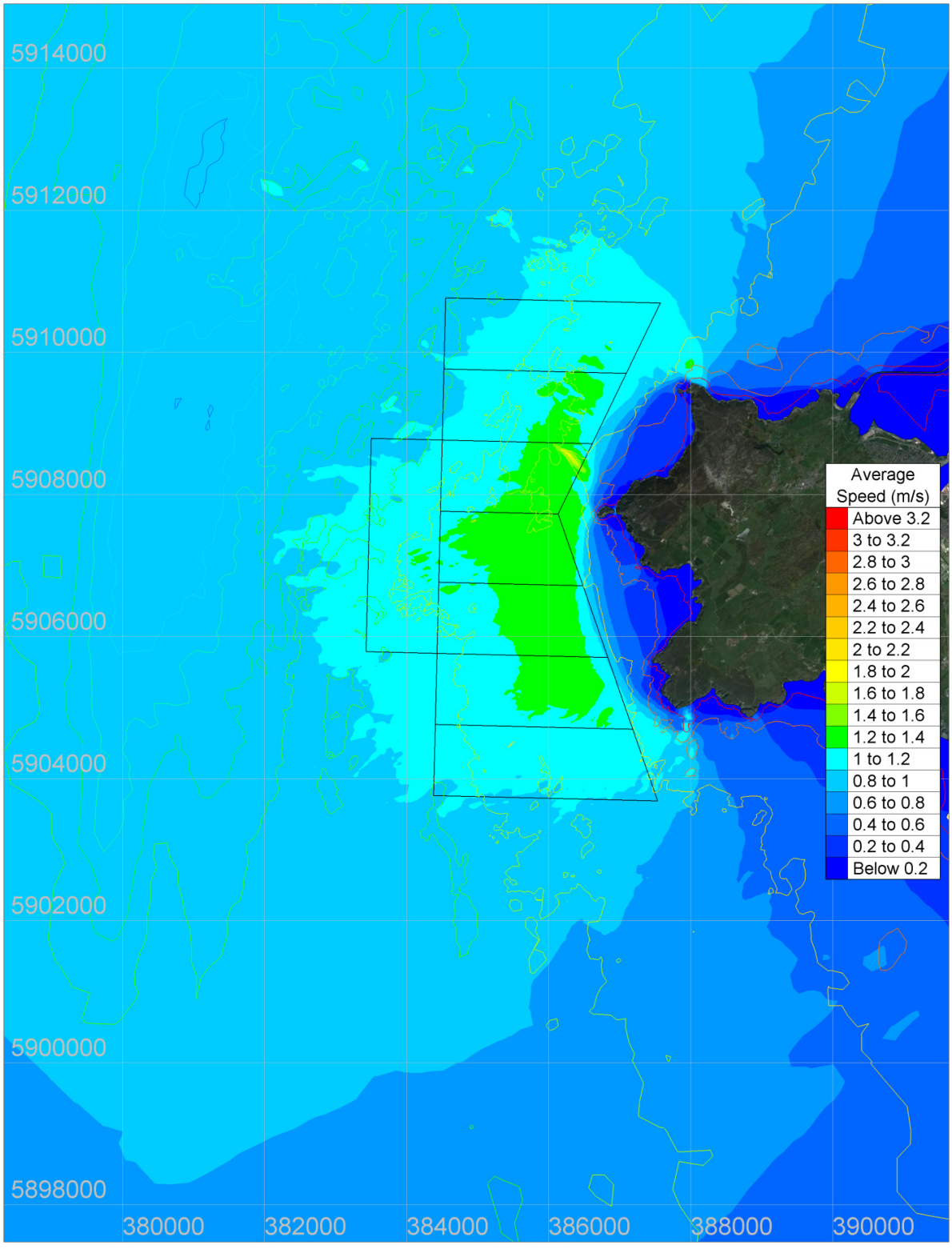

Figure 5.6: Baseline - 29.5 day mean flow speed (m/s)

5.2.2. Scenario 1 (60 MW rated electrical power)

Figure 5.7 below shows the peak depth averaged flow speeds for a mean spring tide range at Holyhead, and Figure 5.8 and Figure 5.9 show changes to peak flood and ebb flows (respectively) for Scenario 1 when compared against the baseline no turbines situation. Figure 5.10 shows the 29.5 day mean flow speed for this scenario.

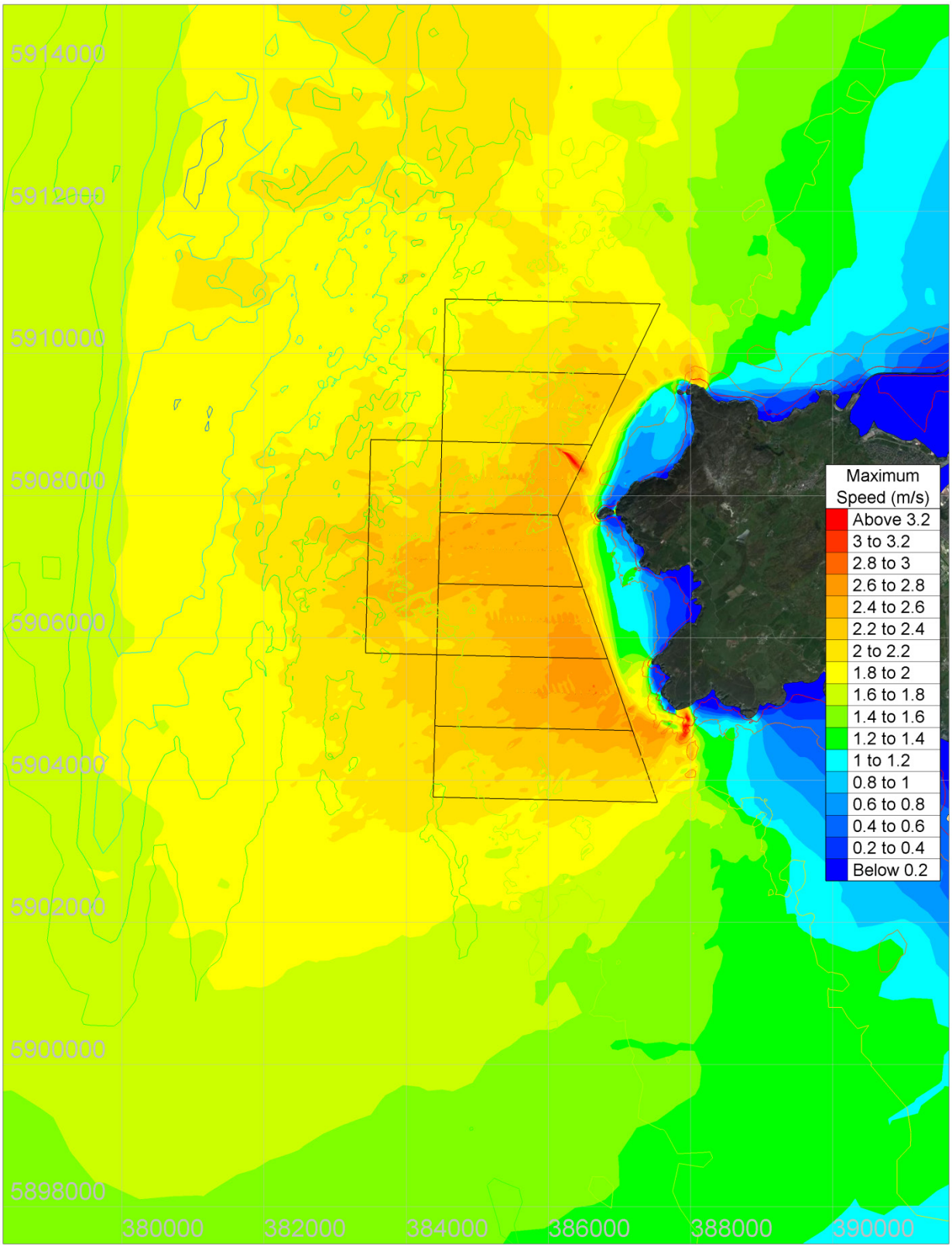

Figure 5.7: Scenario 1 peak flow speed (m/s) for mean spring tide

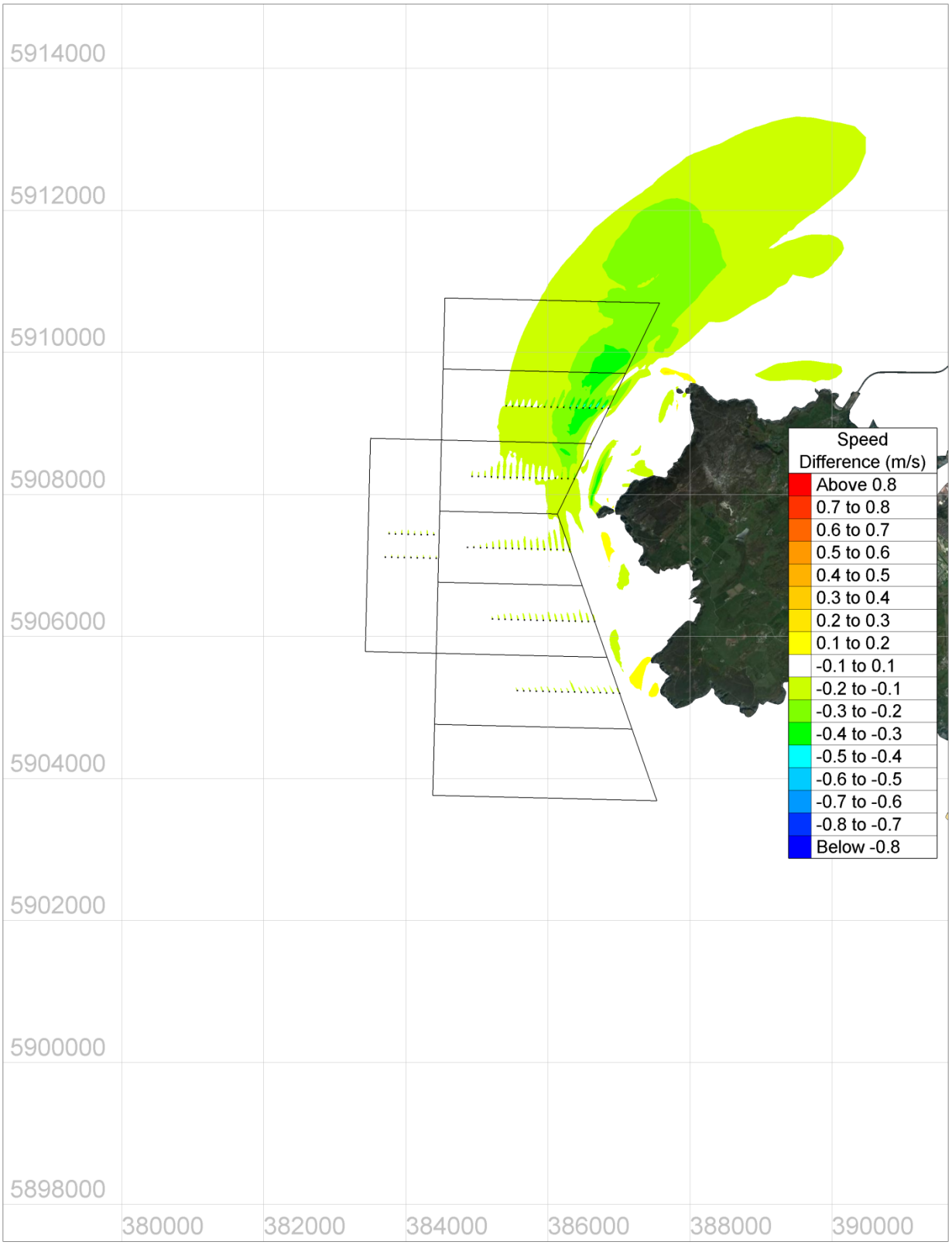

Figure 5.8: Change in mean spring tide peak speed (flood flow, Scenario 1 minus baseline)

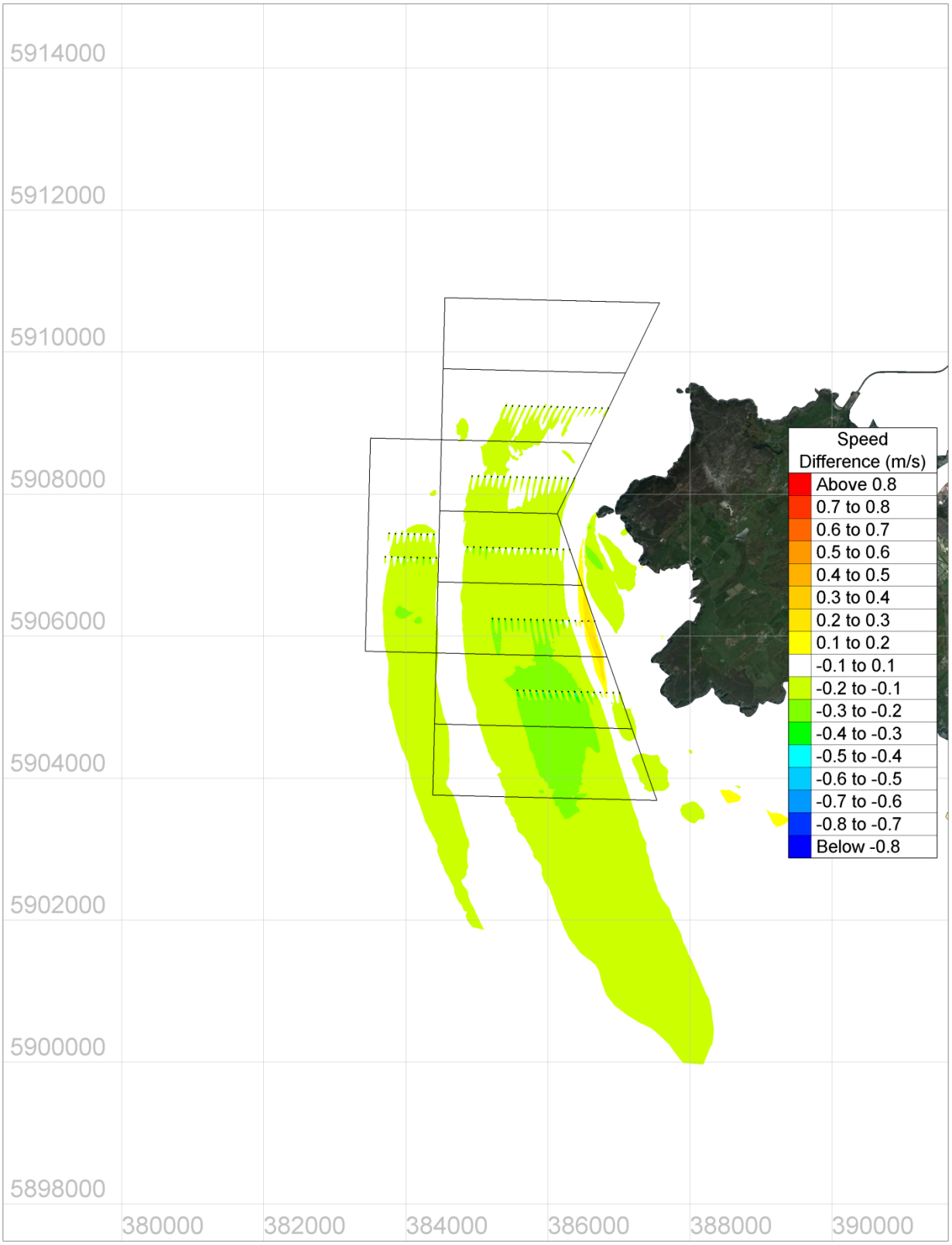

Figure 5.9: Change in mean spring tide peak speed (ebb flow, Scenario 1 minus baseline)

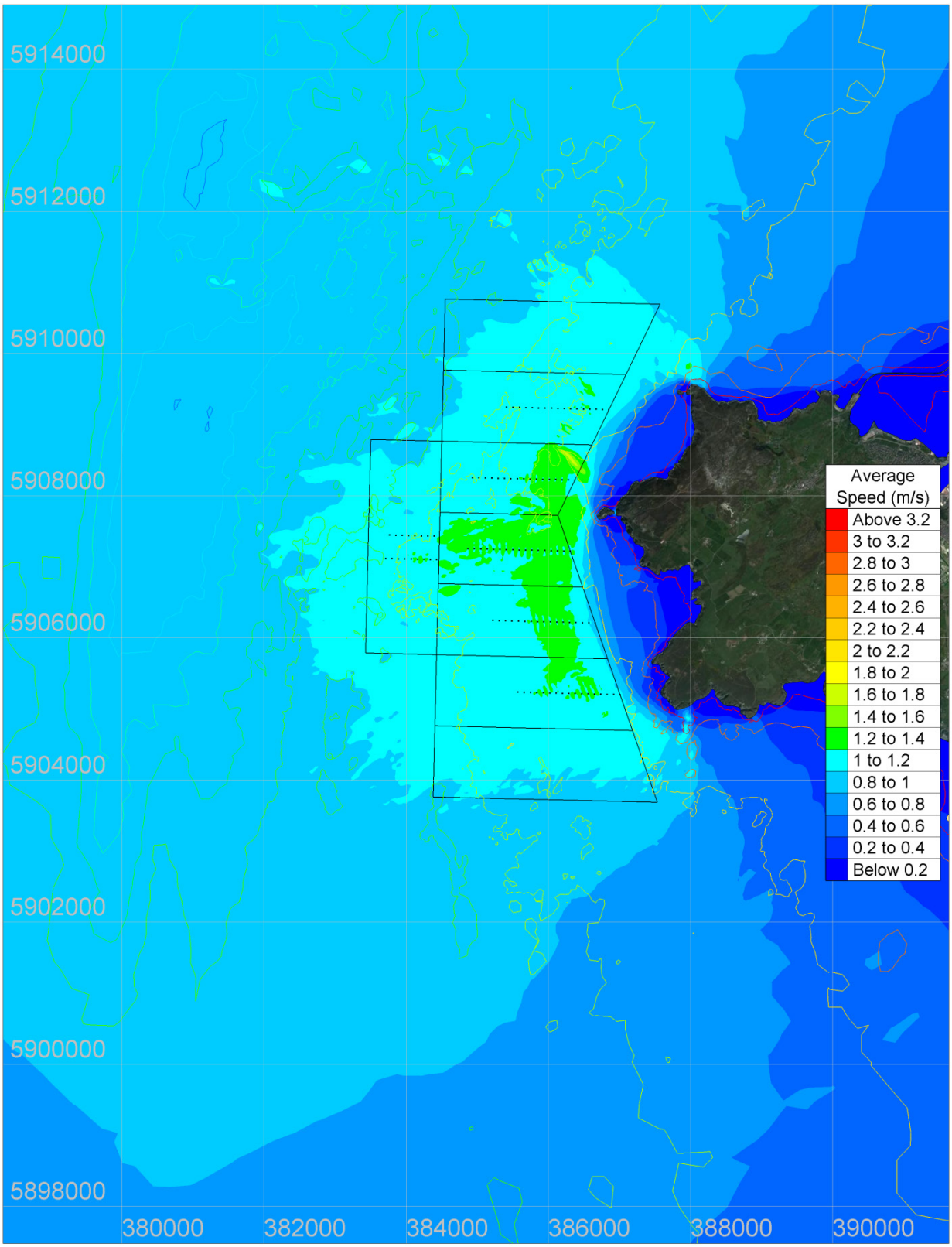

Figure 5.10: Scenario 1 - 29.5 day mean flow speed (m/s)

5.2.3. Scenario 2 (120 MW rated electrical power)

Figure 5.11 below shows the peak depth averaged flow speeds for a mean spring tide range at Holyhead, and Figure 5.12 and Figure 5.13 show changes to peak flood and ebb flows (respectively) for Scenario 2 when compared against the baseline no turbines situation. Figure 5.14 shows the 29.5 day mean flow speed for this scenario.

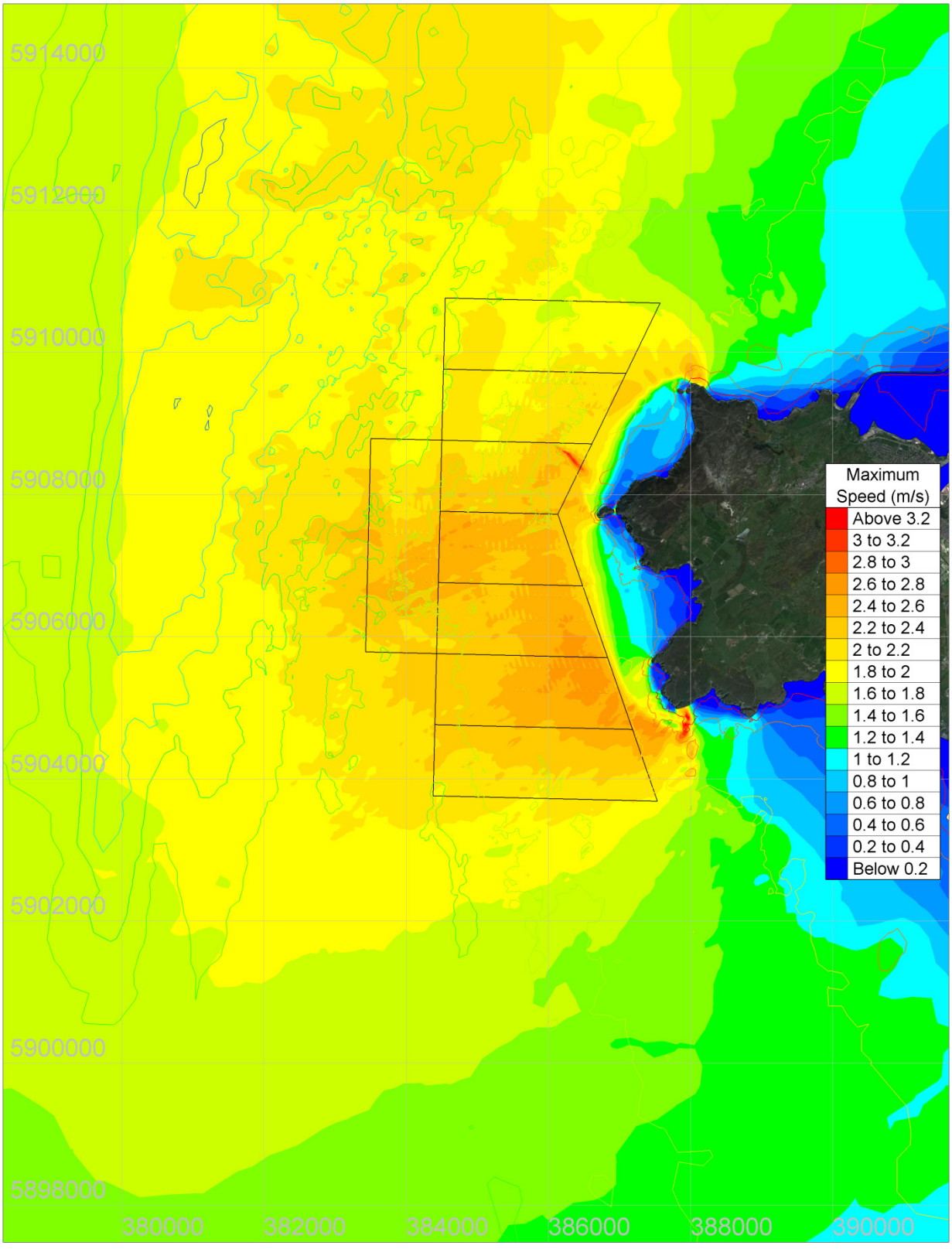

Figure 5.11: Scenario 2 peak flow speed (m/s) for mean spring tide

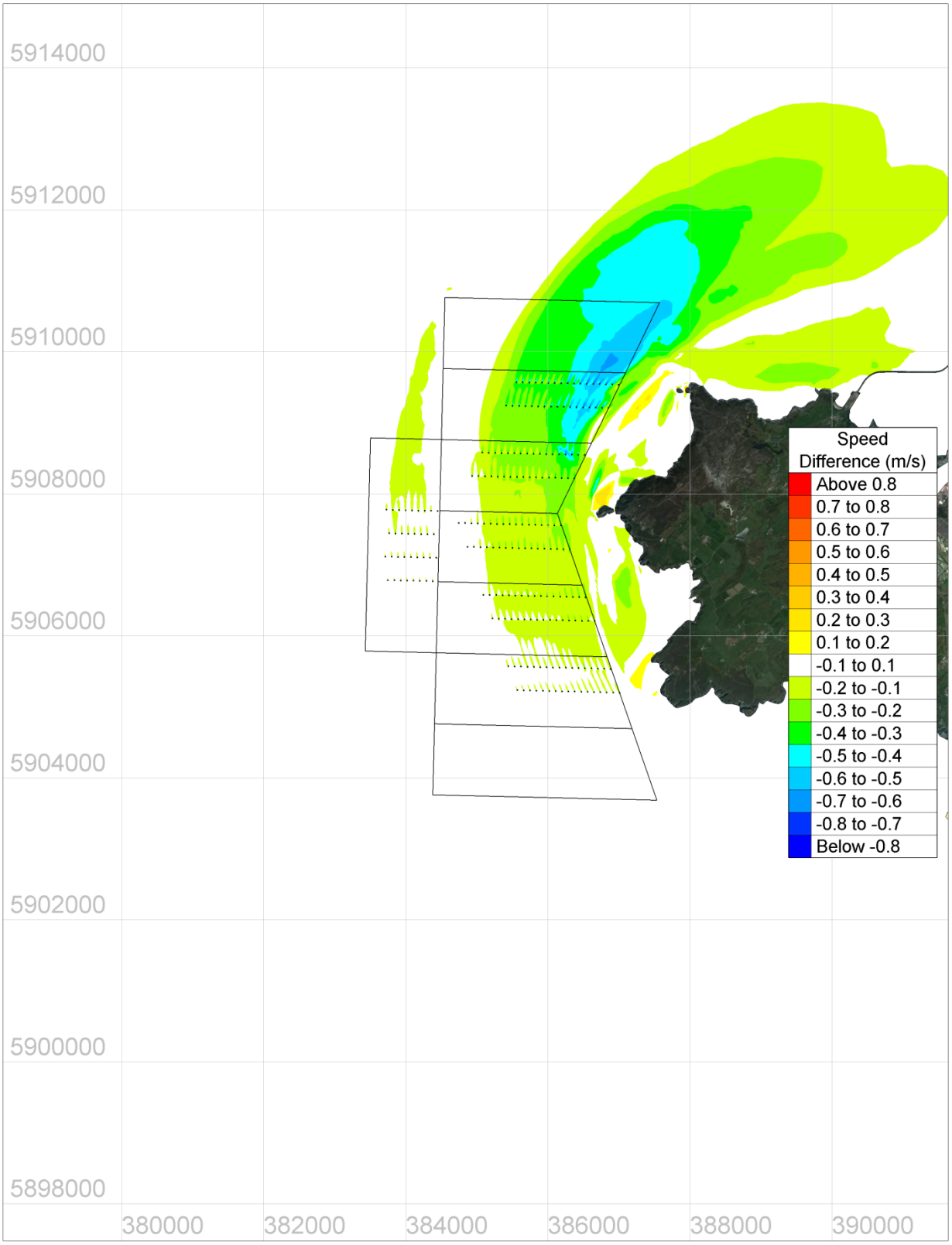

Figure 5.12: Change in mean spring tide peak speed (flood flow, Scenario 2 minus baseline)

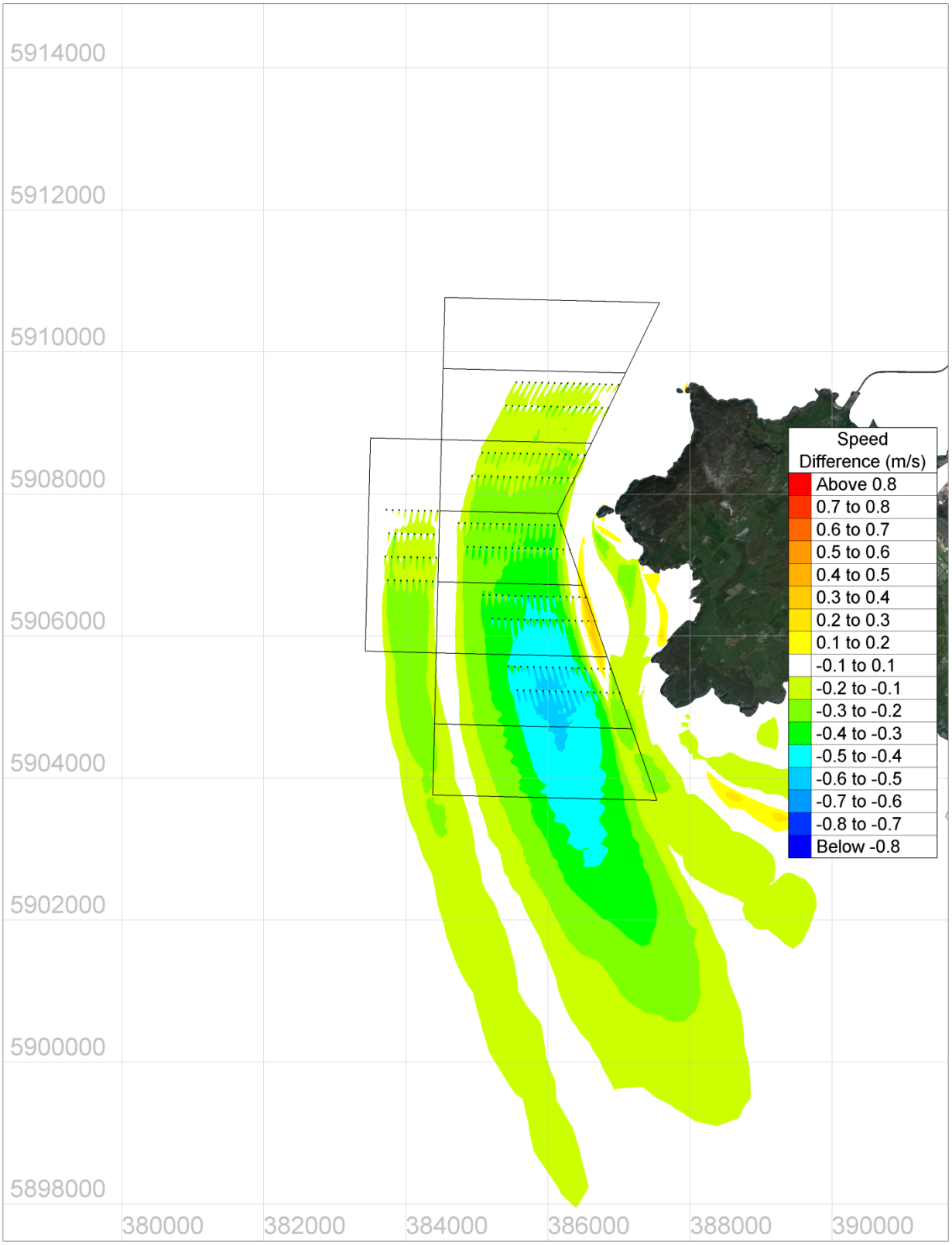

Figure 5.13: Change in mean spring tide peak speed (ebb flow, Scenario 2 minus baseline)

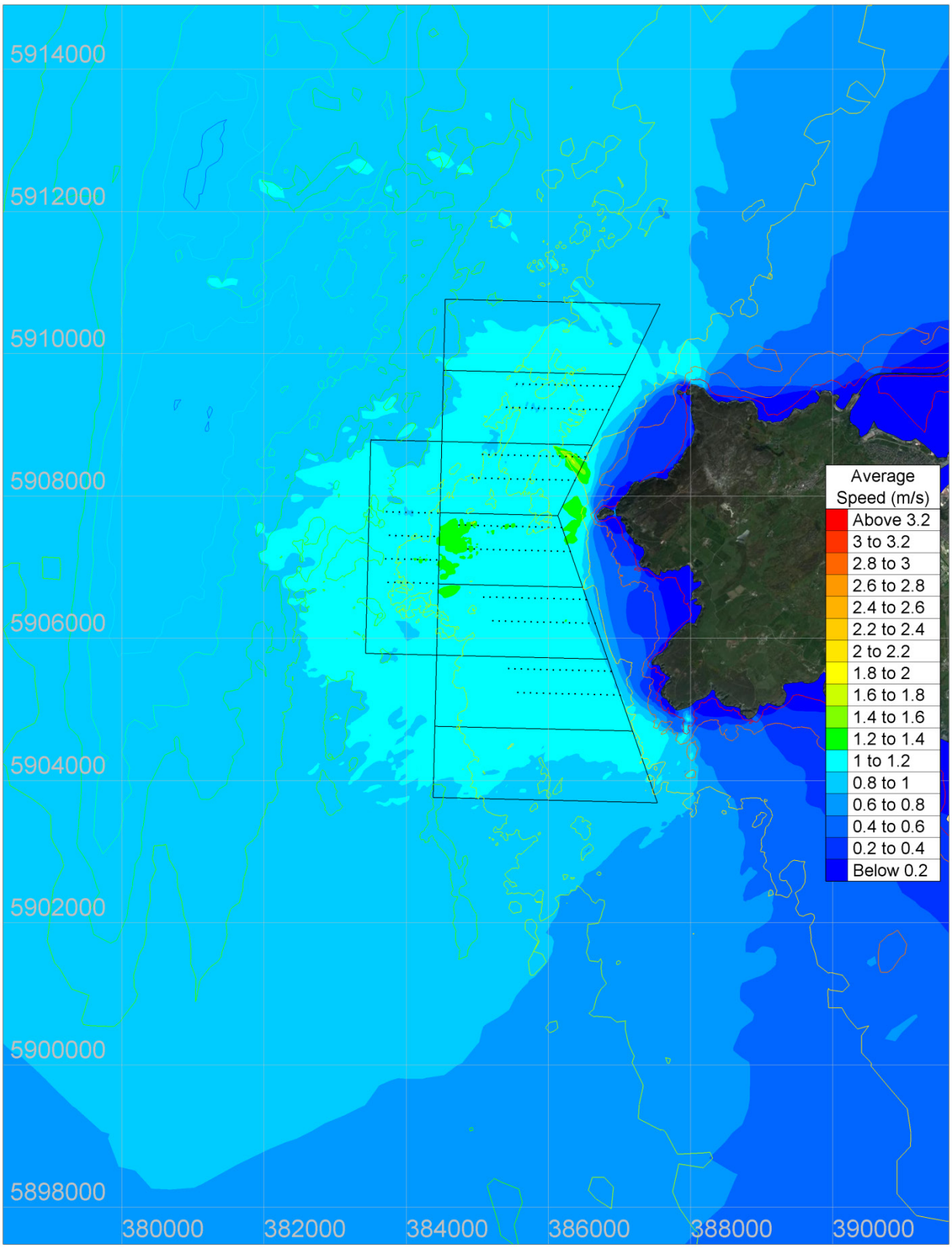

Figure 5.14: Scenario 2 - 29.5 day mean flow speed (m/s)

5.2.4. Scenario 3 (approximately 180 MW rated electrical power)

Figure 5.15 below shows the peak depth averaged flow speeds for a mean spring tide range at Holyhead, and Figure 5.16 and Figure 5.17 show changes to peak flood and ebb flows (respectively) for Scenario 3 when compared against the baseline no turbines situation. Figure 5.18 shows the 29.5 day mean flow speed for this scenario.

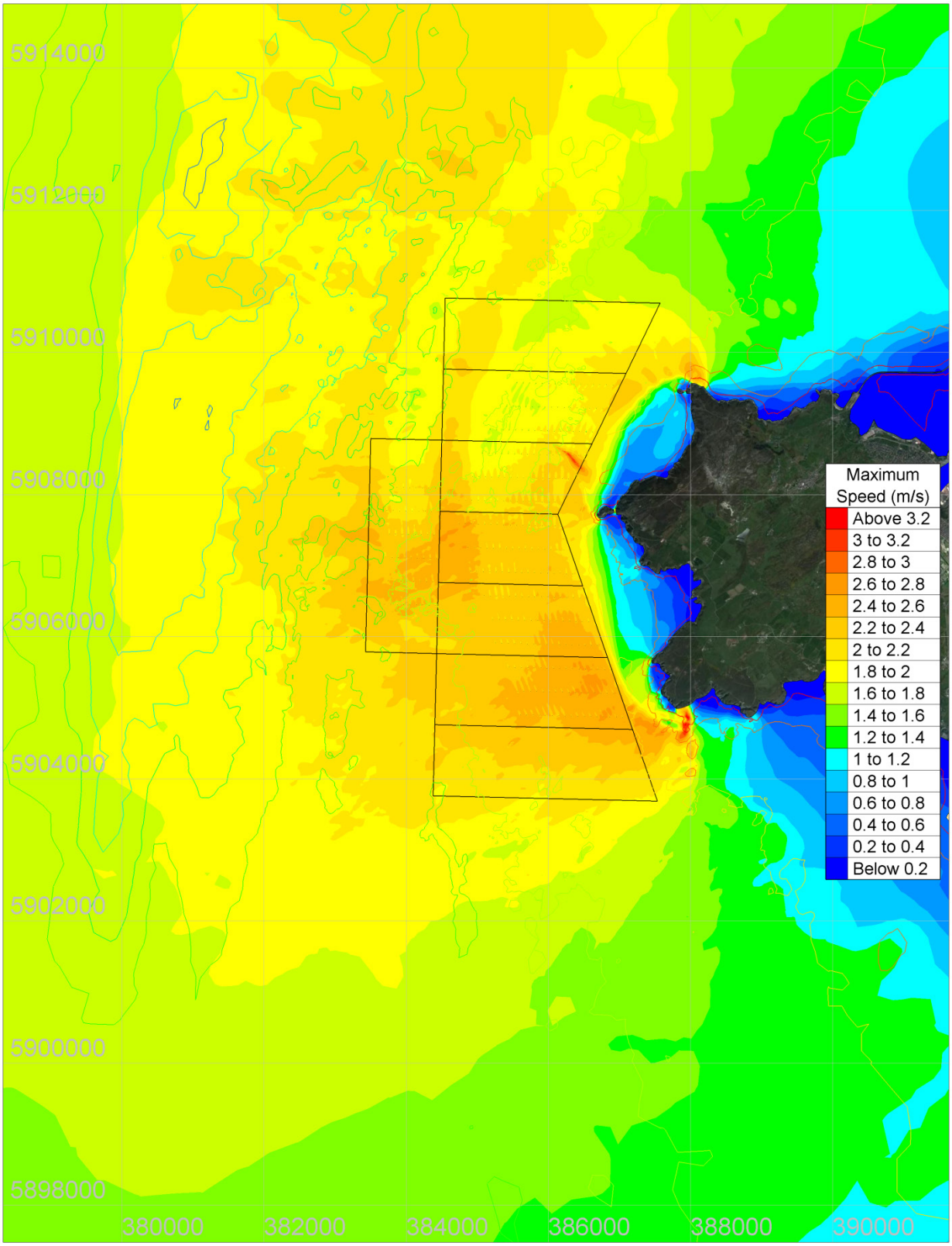

Figure 5.15: Scenario 3 peak flow speed (m/s) for mean spring tide

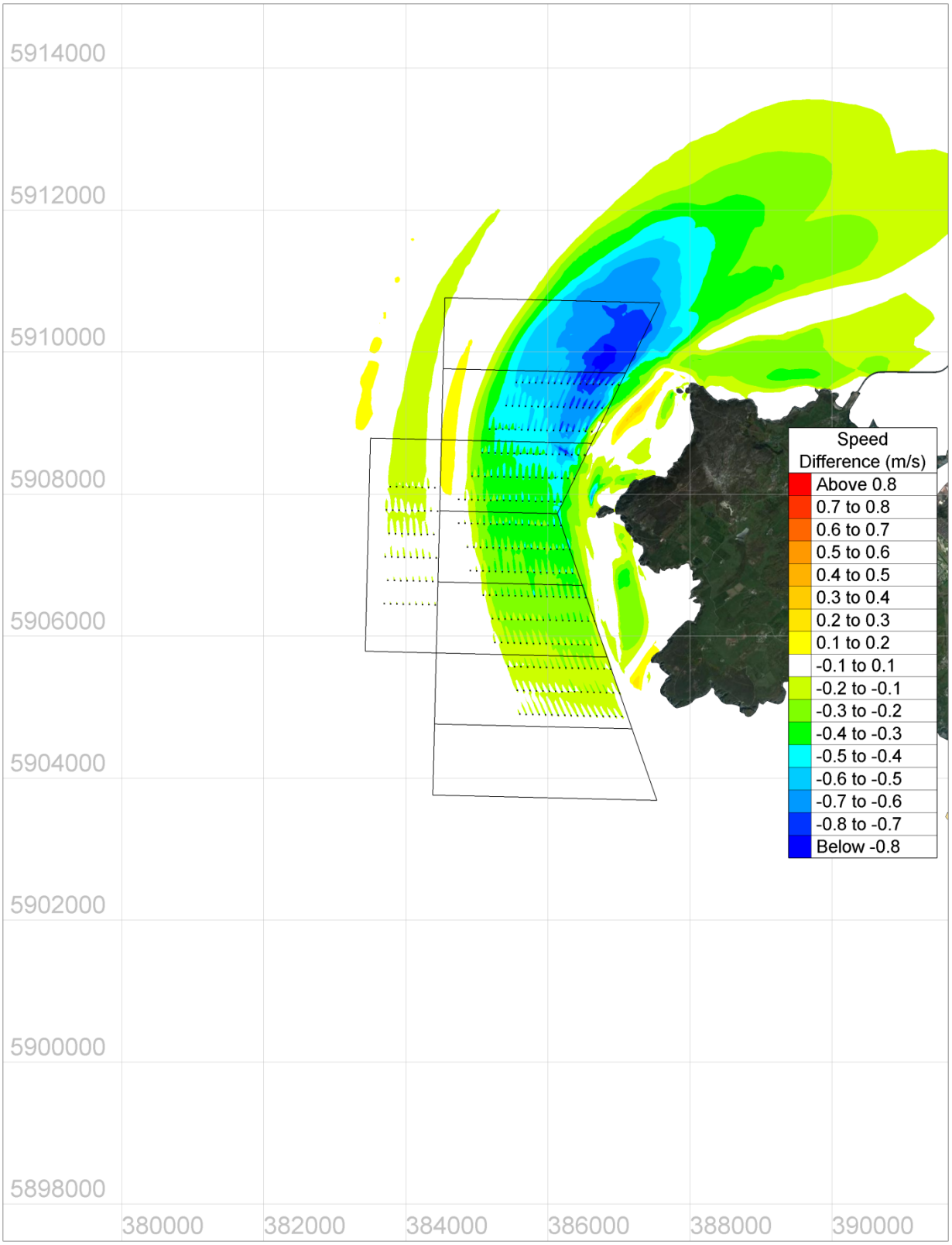

Figure 5.16: Change in mean spring tide peak speed (flood flow, Scenario 3 minus baseline)

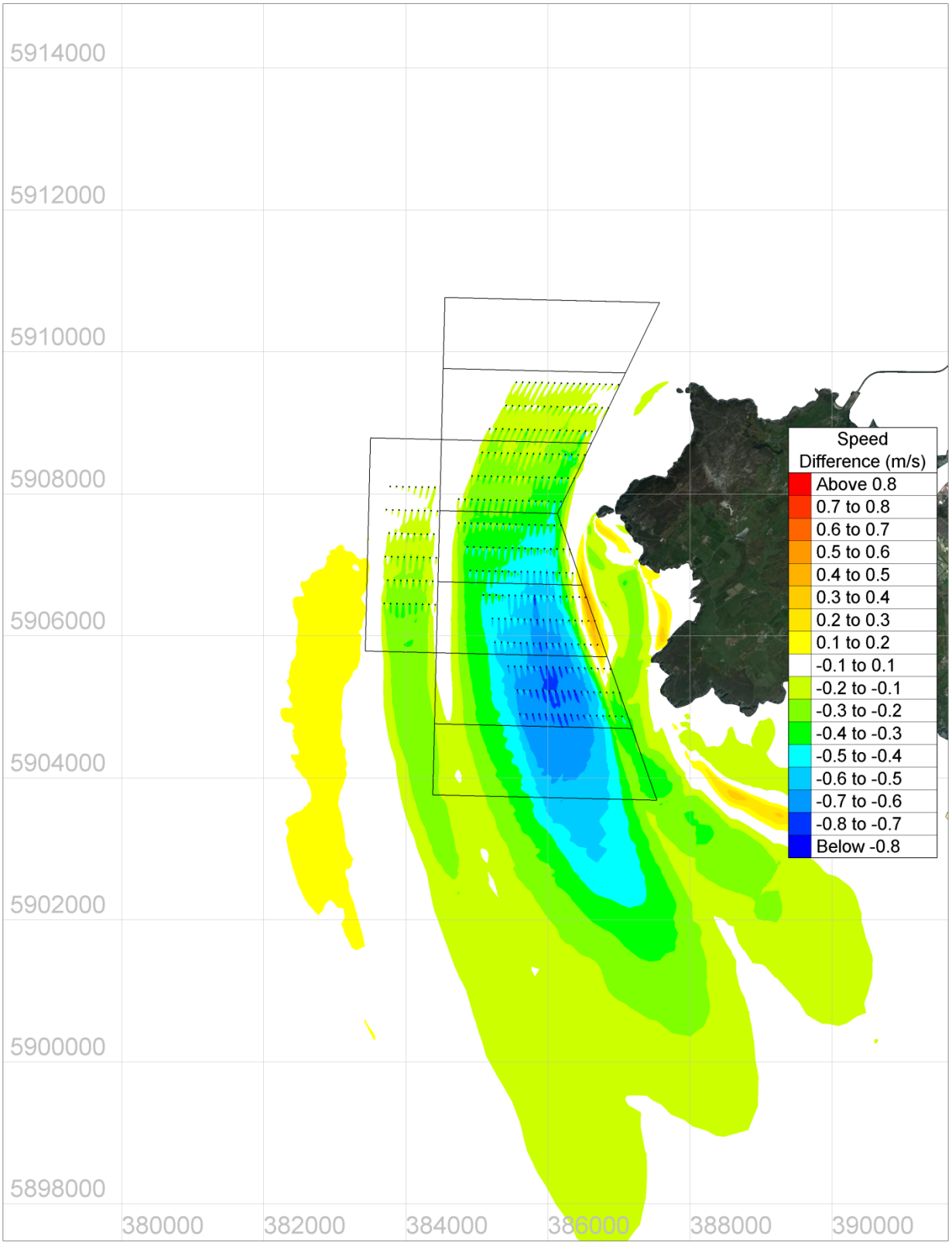

Figure 5.17: Change in mean spring tide peak speed (ebb flow, Scenario 3 minus baseline)

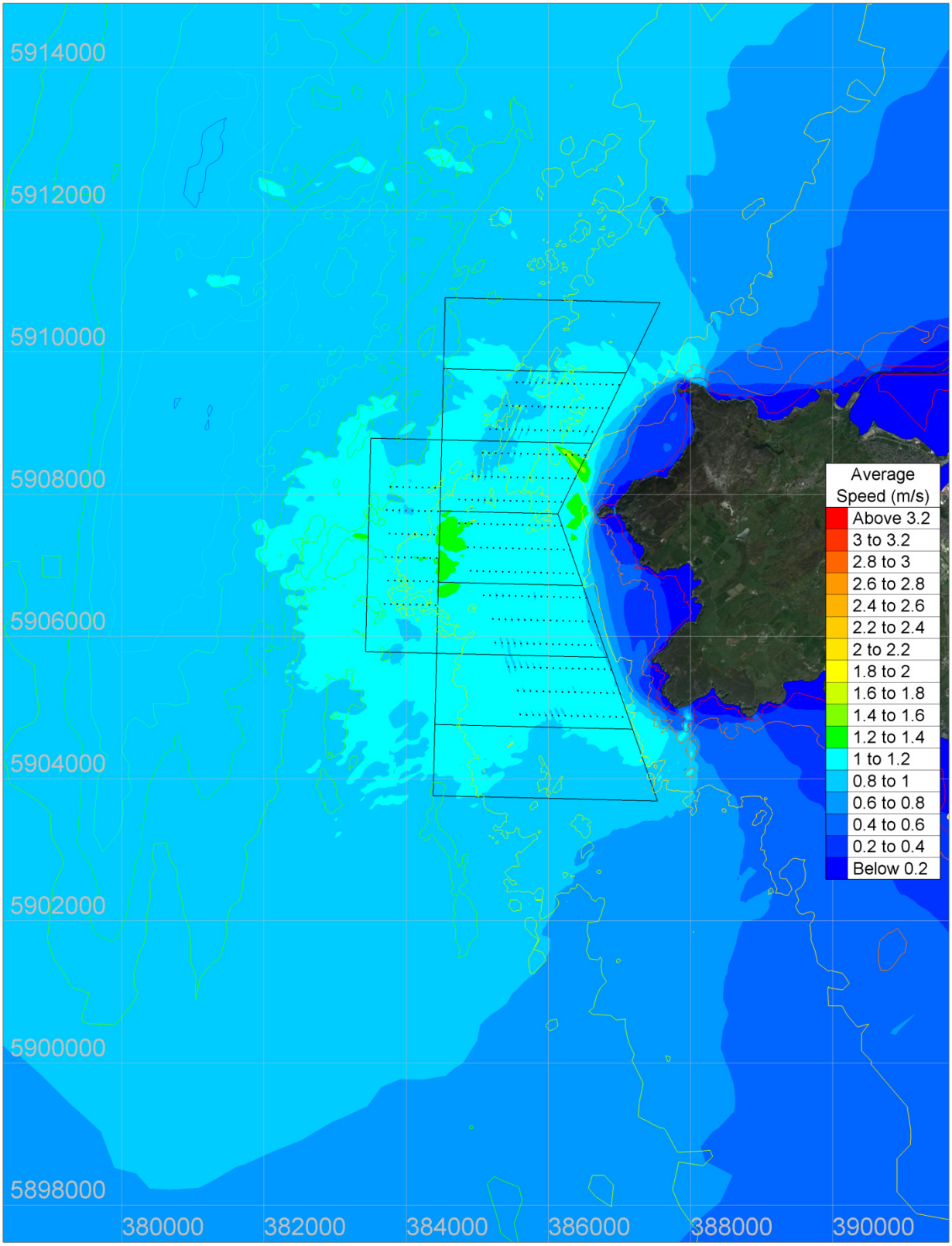

Figure 5.18: Scenario 3 - 29.5 day mean flow speed (m/s)

5.2.5. Scenario 4 (approximately 240 MW rated electrical power)

Figure 5.19 below shows the peak depth averaged flow speeds for a mean spring tide range at Holyhead, and Figure 5.20 and Figure 5.21 show changes to peak flood and ebb flows (respectively) for Scenario 4 when compared against the baseline no turbines situation. Figure 5.22 shows the 29.5 day mean flow speed for this scenario.

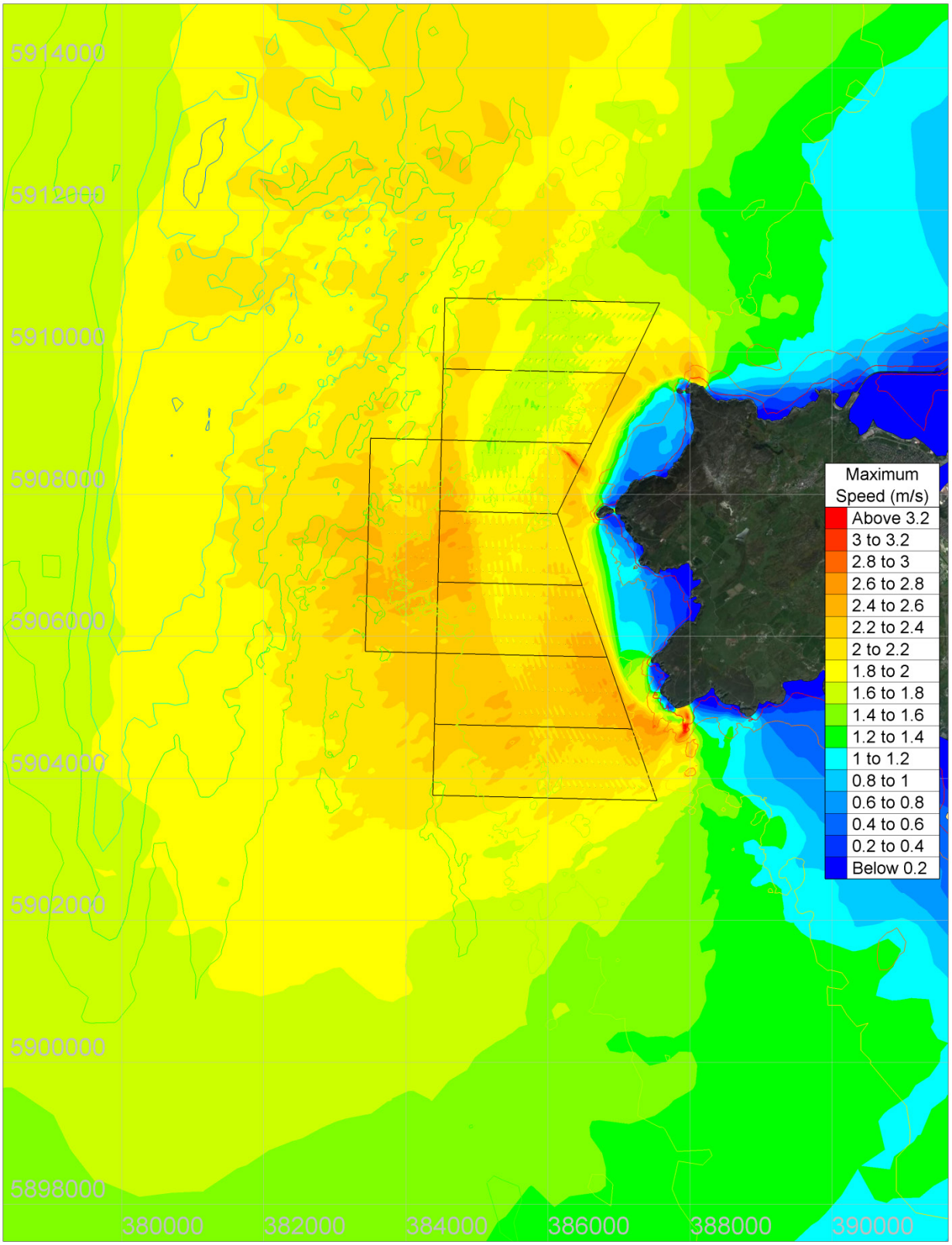

Figure 5.19: Scenario 4 peak flow speed (m/s) for mean spring tide

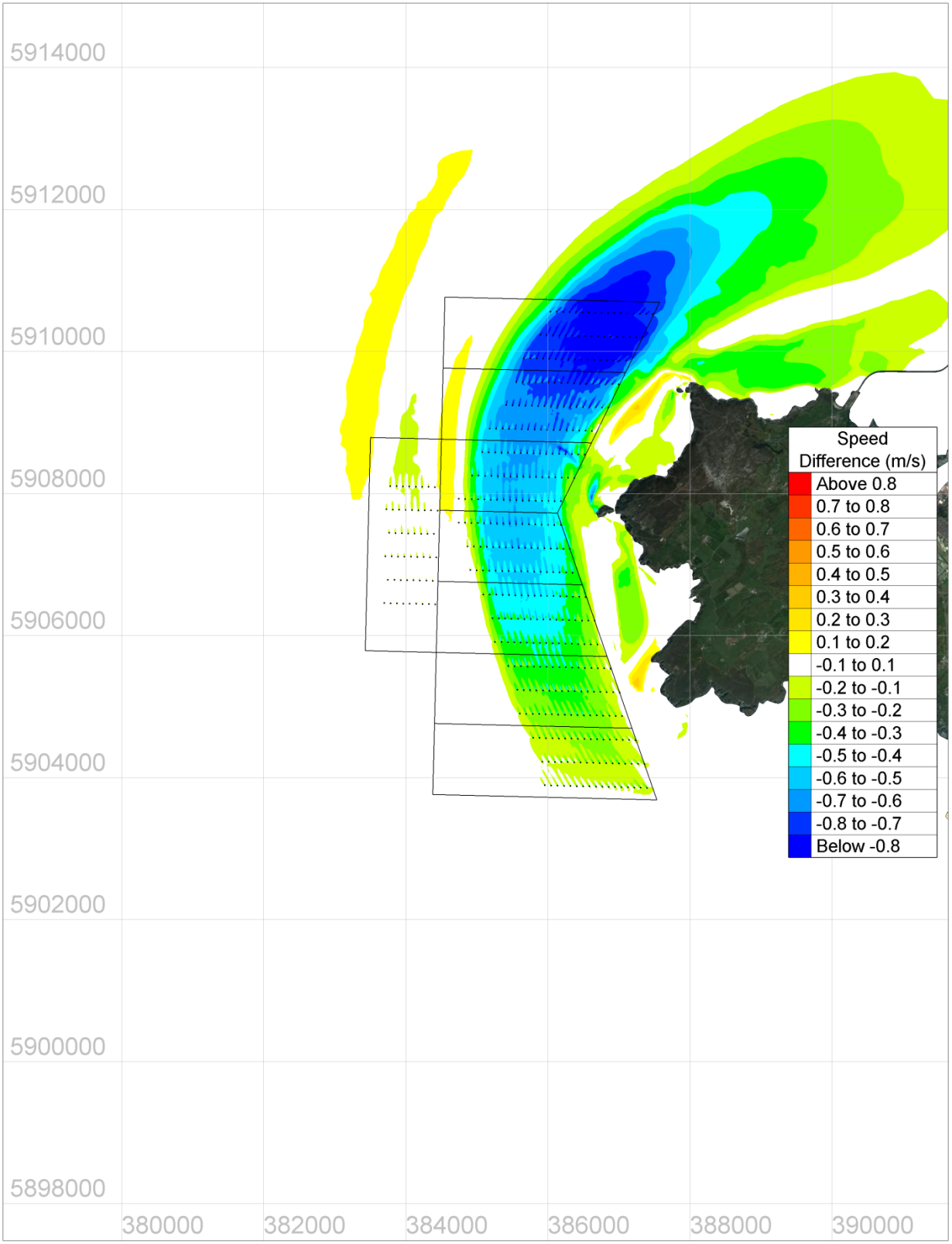

Figure 5.20: Change in mean spring tide peak speed (flood flow, Scenario 4 minus baseline)

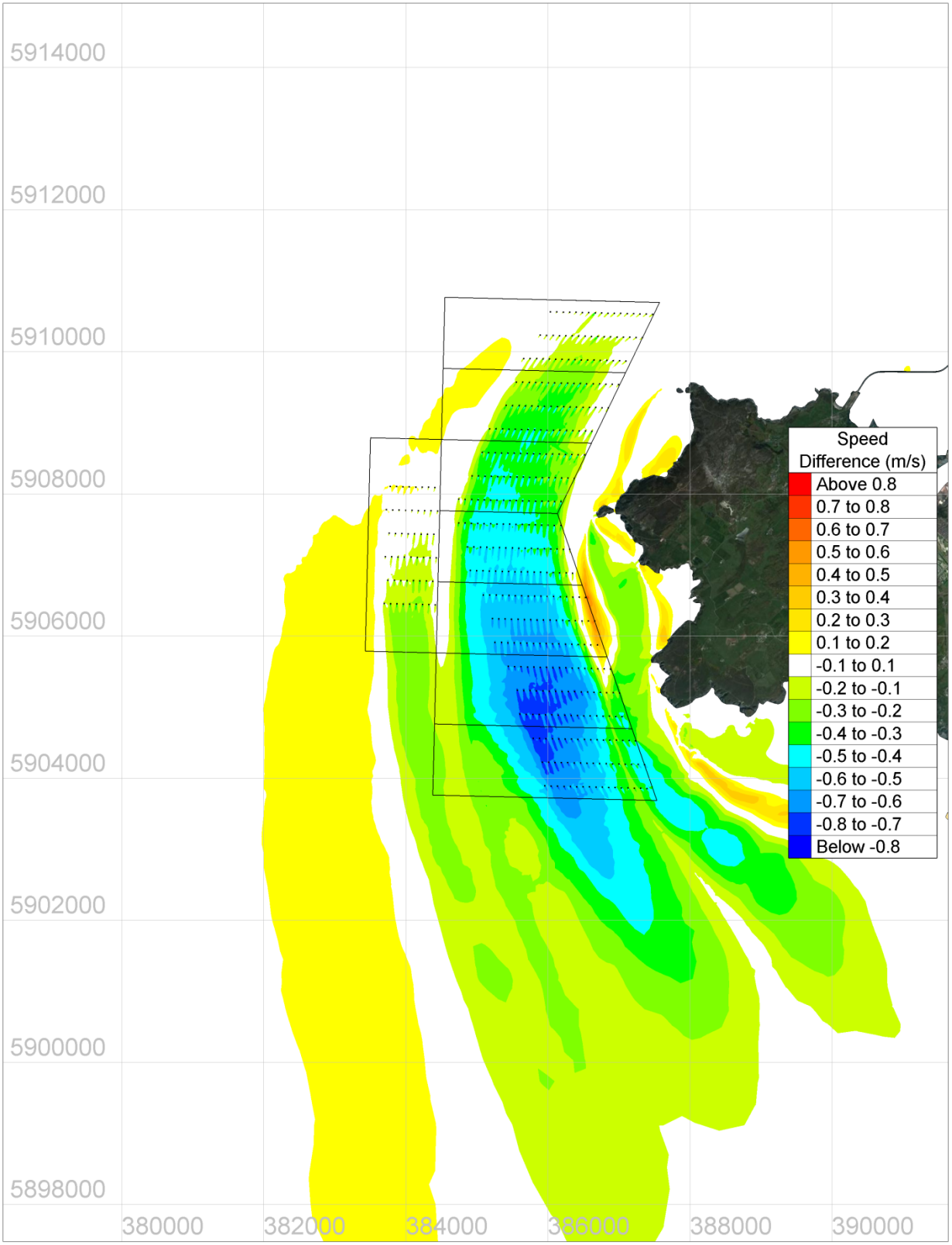

Figure 5.21: Change in mean spring tide peak speed (ebb flow, Scenario 4 minus baseline)

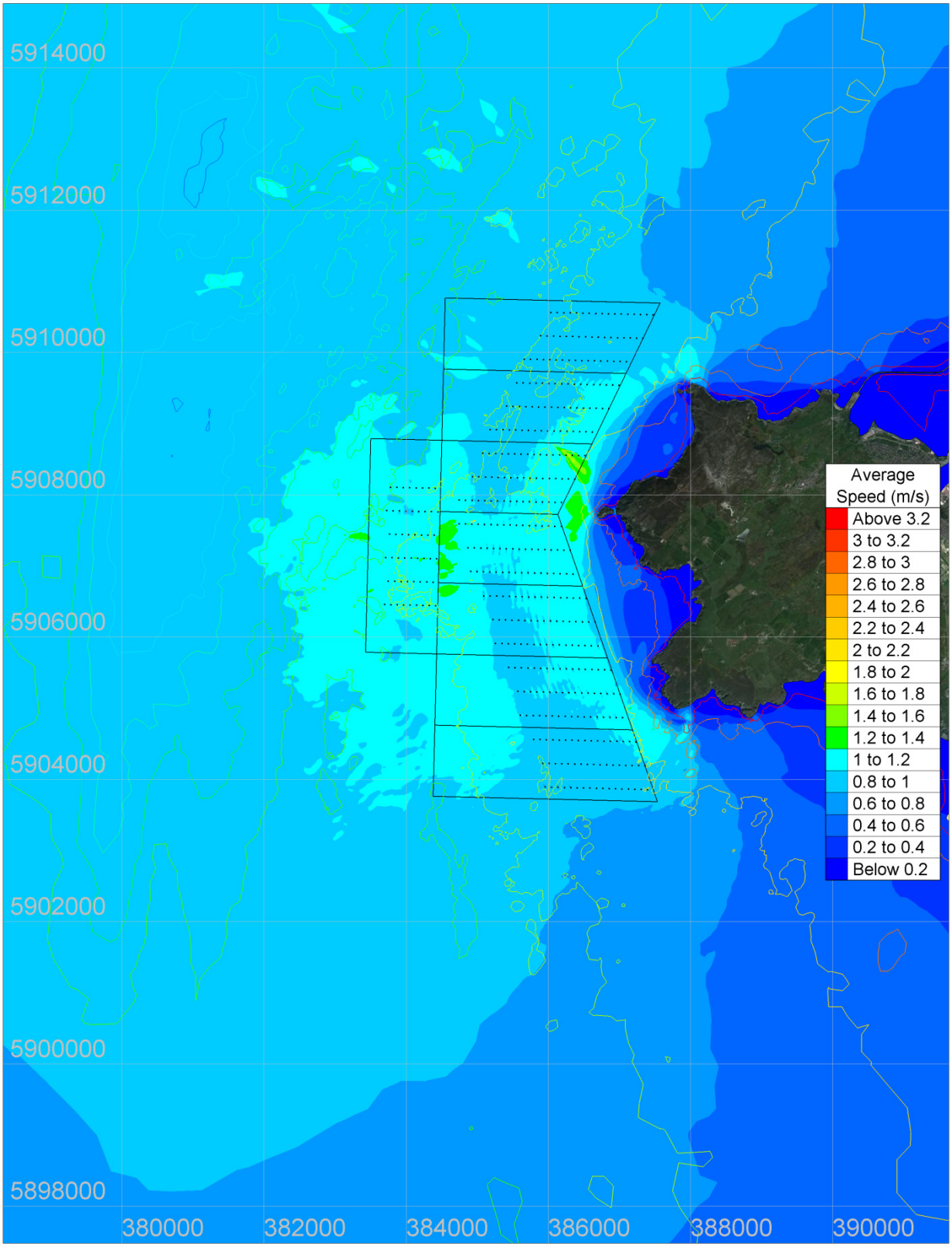

Figure 5.22: Scenario 4 - 29.5 day mean flow speed (m/s)

5.3. Interactions between subzones

For each modelled scenario, outputs are provided for a complete lunar cycle (see separate spreadsheets) at a series of measurement points (100m intervals) along the boundaries of the buffer zones. Outputs include mean velocity, peak velocity, mean spring peak velocity, average power density.

These measurements allow a comparison of the scenarios to comply with the resource assessment standard IEC TS 62600-201:2015. The comparison is on the basis of theoretical extractable power and including a conversion factor to electrical power output provided by Menter Môn.

Measures include mean velocity, peak velocity, mean spring tide peak velocity, and average power density. Figure 5.23 shows the buffer zone line numbers for each of the subzones. Table 5.2 to Table 5.5 show the values of these measures as averaged from the outputs at 100m intervals along each of the buffer zone lines. The 29.5 day values relate to a modelled lunar month and the peak spring tide values are taken from a modelled tide later in the simulation. Section 5.1 describes the extrapolation to a longer term average lunar month.

The effect on these measures of energy extraction by multiple arrays in multiple subzones is clearly seen by comparing these tables.

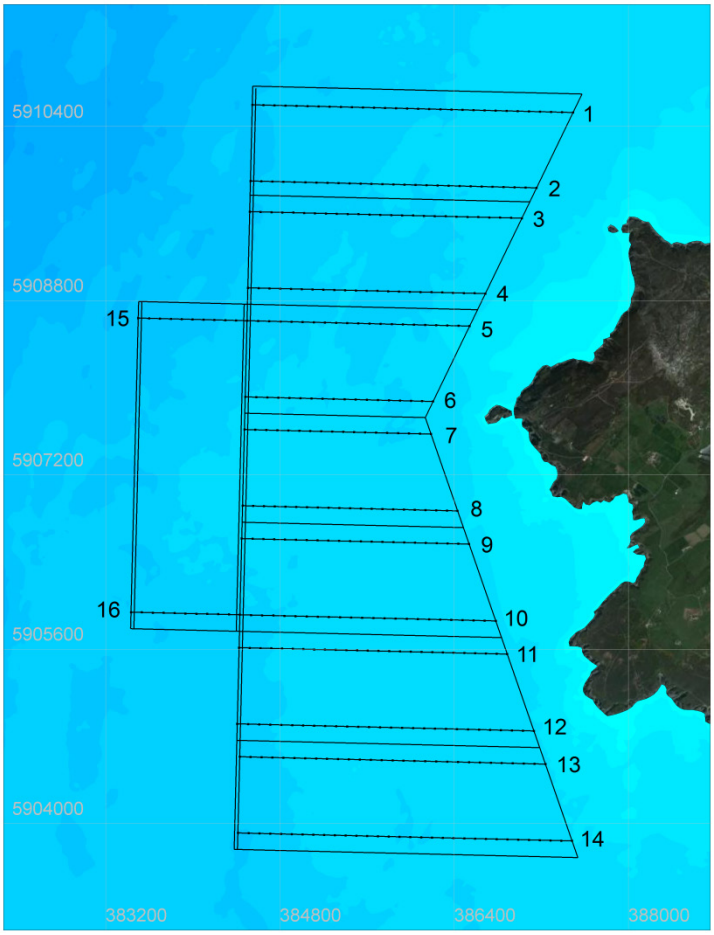

Figure 5.23: Buffer zone line numbers used for assessment of interaction between subzones

Table 5.2: Key modelled measures along buffer zone boundaries (Baseline – no turbines)

Buffer Zone Line No.	29.5 day mean speed (m/s)	29.5 day peak speed (m/s)	Mean spring tide peak speed (m/s)	29.5 day average power density (kW/m^2)
1	1.048	2.126	2.117	1.002
2	1.124	2.300	2.294	1.260
3	1.131	2.329	2.298	1.313
4	1.138	2.317	2.309	1.338
5	1.189	2.419	2.398	1.578
6	1.208	2.455	2.450	1.636
7	1.263	2.568	2.563	1.880
8	1.236	2.525	2.518	1.765
9	1.217	2.520	2.511	1.701
10	1.164	2.471	2.464	1.522
11	1.166	2.484	2.478	1.524
12	1.149	2.451	2.445	1.445
13	1.115	2.376	2.371	1.317
14	1.010	2.126	2.121	0.967
15	0.988	2.063	2.056	0.877
16	1.035	2.211	2.204	1.076

Source: Averaged values of model data extracted at 100m intervals along each buffer zone boundary line shown in Figure 5.23. HR Wallingford.

Table 5.3: Key modelled measures along buffer zone boundaries (Scenario 1)

Buffer Zone Line No.	29.5 day mean speed (m/s)	29.5 day peak speed (m/s)	Mean spring tide peak speed (m/s)	29.5 day average power density (kW/m^2)
1	1.013	2.004	1.996	0.891
2	1.088	2.159	2.150	1.113
3	1.096	2.183	2.175	1.157
4	1.102	2.209	2.202	1.179
5	1.150	2.310	2.304	1.380
6	1.166	2.399	2.395	1.440
7	1.219	2.517	2.512	1.664
8	1.191	2.474	2.468	1.554
9	1.174	2.472	2.465	1.503
10	1.123	2.439	2.434	1.358

Buffer Zone Line No.	29.5 day mean speed (m/s)	29.5 day peak speed (m/s)	Mean spring tide peak speed (m/s)	29.5 day average power density (kW/m^2)
11	1.125	2.457	2.452	1.367
12	1.110	2.441	2.436	1.328
13	1.078	2.369	2.363	1.217
14	0.981	2.122	2.117	0.900
15	0.987	2.038	2.032	0.860
16	1.030	2.213	2.206	1.058

Source: Averaged values of model data extracted at 100m intervals along each buffer zone boundary line shown in Figure 5.23. HR Wallingford.

Table 5.4: Key modelled measures along buffer zone boundaries (Scenario 2)

Buffer Zone Line No.	29.5 day mean speed (m/s)	29.5 day peak speed (m/s)	Mean spring tide peak speed (m/s)	29.5 day average power density (kW/m^2)
1	0.978	1.891	1.884	0.801
2	1.051	2.041	2.034	0.991
3	1.056	2.066	2.061	1.019
4	1.064	2.118	2.111	1.036
5	1.102	2.219	2.212	1.184
6	1.120	2.333	2.329	1.262
7	1.170	2.452	2.447	1.467
8	1.145	2.421	2.414	1.374
9	1.126	2.413	2.405	1.328
10	1.085	2.406	2.401	1.223
11	1.081	2.420	2.415	1.227
12	1.079	2.429	2.424	1.247
13	1.051	2.360	2.354	1.148
14	0.960	2.117	2.111	0.856
15	0.986	2.009	2.003	0.852
16	1.024	2.213	2.206	1.041

Source: Averaged values of model data extracted at 100m intervals along each buffer zone boundary line shown in Figure 5.23. HR Wallingford.

Table 5.5: Key modelled measures along buffer zone boundaries (Scenario 3)

Buffer Zone Line No.	29.5 day mean speed (m/s)	29.5 day peak speed (m/s)	Mean spring tide peak speed (m/s)	29.5 day average power density (kW/m^2)
1	0.946	1.880	1.873	0.739
2	1.018	1.998	1.992	0.904
3	1.025	1.999	1.993	0.926
4	1.037	1.999	1.991	0.947
5	1.067	2.093	2.086	1.053
6	1.077	2.216	2.209	1.110
7	1.125	2.341	2.333	1.289
8	1.104	2.334	2.326	1.226
9	1.084	2.332	2.324	1.178
10	1.048	2.350	2.344	1.100
11	1.044	2.370	2.364	1.109
12	1.052	2.404	2.397	1.179
13	1.027	2.338	2.331	1.091
14	0.941	2.103	2.097	0.822
15	0.986	1.999	1.993	0.850
16	1.024	2.215	2.208	1.041

Source: Averaged values of model data extracted at 100m intervals along each buffer zone boundary line shown in Figure 5.23. HR Wallingford.

Table 5.6: Key modelled measures along buffer zone boundaries (Scenario 4)

Buffer Zone Line No.	29.5 day mean speed (m/s)	29.5 day peak speed (m/s)	Mean spring tide peak speed (m/s)	29.5 day average power density (kW/m^2)
1	0.902	1.854	1.847	0.664
2	0.962	1.931	1.924	0.790
3	0.970	1.930	1.923	0.806
4	0.996	1.914	1.907	0.844
5	1.030	1.989	1.984	0.952
6	1.038	2.082	2.074	0.985
7	1.085	2.198	2.190	1.143
8	1.073	2.221	2.211	1.113
9	1.053	2.228	2.217	1.067

Buffer Zone Line No.	29.5 day mean speed (m/s)	29.5 day peak speed (m/s)	Mean spring tide peak speed (m/s)	29.5 day average power density (kW/m^2)
10	1.019	2.267	2.259	0.999
11	1.015	2.292	2.285	1.006
12	1.019	2.334	2.328	1.069
13	0.990	2.269	2.263	0.985
14	0.920	2.092	2.086	0.797
15	0.989	2.040	2.036	0.875
16	1.028	2.238	2.233	1.059

Source: Averaged values of model data extracted at 100m intervals along each buffer zone boundary line shown in Figure 5.23. HR Wallingford.

6. Conclusions and recommendations

A very high resolution 2D finite element model has been applied to simulate the effects of four scenarios, with installed capacities of 60MW, 120MW, approximately 180MW and approximately 240MW of tide stream devices and assess the potential interactions between subzones in accordance with IEC TS 62600-201:2015. Up to 408 turbines have been modelled and the potential resource extraction and resulting effects on flow speeds and average power density have been assessed.

The following represent some of the main assumptions in the work completed, and it is recommended that the potential interactions between subzones are reassessed when the time comes where less generic, more specific arrays of specific devices are being proposed, perhaps utilising the increased power potential of the eastern sides of some of the sub zones.

- Array design (the purpose of this study has not been to optimise array design) e.g. location and spacing / density of turbines. Optimisation of array design to minimise interaction may lead to increased peak power yield for Scenarios 3 and 4;
- Thrust and power curves for “generic” turbine device and support structure;
- Meteorological effects (waves and storm surge);
- The turbines were assumed to yaw with the current direction.

HR Wallingford
Working with water

HR Wallingford is an independent engineering and environmental hydraulics organisation. We deliver practical solutions to the complex water-related challenges faced by our international clients. A dynamic research programme underpins all that we do and keeps us at the leading edge. Our unique mix of know-how, assets and facilities includes state of the art physical modelling laboratories, a full range of numerical modelling tools and, above all, enthusiastic people with world-renowned skills and expertise.

HR Wallingford, Howbery Park, Wallingford, Oxfordshire OX10 8BA, United Kingdom
tel +44 (0)1491 835381 fax +44 (0)1491 832233 email info@hrwallingford.com
www.hrwallingford.com

FS 516431
EMS 558310
OHS 595357